A Global Synthesis Inversion Analysis of Recent Variability in CO_2 Fluxes Using GOSAT and In Situ Observations

James S. Wang,[1,2] S. Randolph Kawa,[2] G. James Collatz,[2] Motoki Sasakawa,[3] Luciana V. Gatti,[4] Toshinobu Machida,[3] Yuping Liu,[5,2] and Michael E. Manyin[5,2]

[1]Universities Space Research Association, Columbia, MD, USA, james.s.wang@nasa.gov

[2]NASA Goddard Space Flight Center, Greenbelt, MD, USA

[3]National Institute for Environmental Studies, Center for Global Environmental Research, Ibaraki, Tsukuba Onogawa, Japan

[4]Instituto de Pesquisas Energéticas e Nucleares (IPEN)–Comissao Nacional de Energia Nuclear (CNEN), Sao Paulo, Brazil

[5]Science Systems and Applications, Inc., Lanham, MD, USA

Submitted to Atmospheric Chemistry and Physics (as part of Special Issue "The 10th International Carbon Dioxide Conference (ICDC10) and the 19th WMO/IAEA Meeting on Carbon Dioxide, other Greenhouse Gases and Related Measurement Techniques (GGMT-2017)")

Abstract

The precise contribution of the two major sinks for anthropogenic CO_2 emissions, terrestrial vegetation and the ocean, and their location and year-to-year variability are not well understood. Top-down estimates of the spatiotemporal variations in emissions and uptake of CO_2 are expected to benefit from the increasing measurement density brought by recent in situ and remote CO_2 observations. We uniquely apply a batch Bayesian synthesis inversion at relatively high resolution to in situ surface observations and bias-corrected GOSAT satellite column CO_2 retrievals to deduce the global distributions of natural CO_2 fluxes during 2009-2010. Our objectives include evaluating bottom-up prior flux estimates, assessing the value added by the satellite data, and examining the impacts of inversion technique and assumptions on posterior fluxes and uncertainties. The GOSAT inversion is generally better constrained than the in situ inversion, with smaller posterior regional flux uncertainties and correlations, because of greater spatial coverage, except over North America and northern and southern high-latitude ocean. Complementarity of the in situ and GOSAT data enhances uncertainty reductions in a joint inversion; however, remaining coverage gaps, including those associated with spatial and temporal sampling biases in the passive satellite measurements, still limit the ability to accurately resolve fluxes down to the sub-continental/sub-ocean basin scale. The GOSAT inversion produces a shift in the global CO_2 sink from the tropics to the north and south relative to the prior, and an increased source in the tropics of ~2 Pg C y^{-1} relative to the in situ inversion, similar to what is seen in studies using other inversion approaches. This result may be driven by sampling and residual retrieval biases in the GOSAT data, as suggested by significant discrepancies between posterior CO_2 distributions and surface in situ and HIPPO mission aircraft data. While the shift in the global sink appears to be a robust feature of the inversions, the

47 partitioning of the sink between land and ocean in the inversions using either in situ or GOSAT
48 data is found to be sensitive to prior uncertainties because of negative correlations in the flux
49 errors. The GOSAT inversion indicates significantly less CO_2 uptake in summer of 2010 than in
50 2009 across northern regions, consistent with the impact of observed severe heat waves and
51 drought. However, observations from an in situ network in Siberia imply that the GOSAT
52 inversion exaggerates the 2010-2009 difference in uptake in that region, while the prior CASA-
53 GFED model of net ecosystem production and fire emissions reasonably estimates that quantity.
54 The prior, in situ posterior, and GOSAT posterior all indicate greater uptake over North America
55 in spring to early summer of 2010 than in 2009, consistent with wetter conditions. The GOSAT
56 inversion does not show the expected impact on fluxes of a 2010 drought in the Amazon;
57 evaluation of posterior mole fractions against local aircraft profiles suggests that time-varying
58 GOSAT coverage can bias estimation of flux interannual variability in this region.
59

1. Introduction

About one-half of the global CO_2 emissions from fossil fuel combustion and deforestation accumulates in the atmosphere (Le Quéré et al., 2015), where it contributes to global climate change. The rest is taken up by land vegetation and the ocean. The precise contribution of the two sinks, their location and year-to-year variability, and the environmental controls on the variability are, however, not well understood. Top-down methods involving atmospheric inverse modeling have been used extensively to quantify natural CO_2 fluxes (e.g. Enting and Mansbridge, 1989; Ciais et al., 2010). An advantage of this approach over bottom-up methods such as forest inventories (Pan et al., 2011; Hayes et al., 2012) or direct flux measurements (Baldocchi et al., 2001; Chevallier et al., 2012) is that measurements of atmospheric CO_2 mole fractions generally contain the influence of fluxes over a spatial scale substantially larger than that of individual forest plots or flux measurements, so that errors from extrapolating measurements to climatically relevant scales (e.g. ecosystem, sub-continental, or global) are mitigated. However, the accuracy of top-down methods is limited by incomplete data coverage (especially for highly precise but sparse in situ observation networks), uncertainties in atmospheric transport modeling, and mixing of signals from different flux types such as anthropogenic and natural.

With the advent of retrievals of atmospheric CO_2 mole fraction from satellites, including the Japanese Greenhouse gases Observing SATellite (GOSAT) (Yokota et al., 2009) and the NASA Orbiting Carbon Observatory-2 (OCO-2) (Crisp, 2015; Eldering et al., 2017), data coverage has improved substantially. Making measurements since 2009, GOSAT is the first satellite in orbit designed specifically to measure column mixing ratios of CO_2 (as well as methane) with substantial sensitivity to the lower troposphere, close to surface fluxes. A number

of modeling groups have conducted CO_2 flux inversions using synthetic GOSAT data (Liu et al., 2014) and actual data (Takagi et al., 2011; Maksyutov et al., 2013; Basu et al., 2013; Saeki et al., 2013a; Deng et al., 2014; Chevallier et al., 2014; Takagi et al., 2014; Reuter et al., 2014; Houweling et al., 2015; Deng et al., 2016). Unlike in situ measurements, which are calibrated directly for the gas of interest, remote sensing involves challenges in precision and accuracy stemming from the measuring of radiance. The retrievals rely on modeling of radiative transfer involving complicated absorption and scattering by the atmosphere and reflection from the surface (e.g. Connor et al., 2008; O'Dell et al., 2012). Passive measurements that rely on reflected sunlight are more prone to errors than active measurements, as they are affected by not only errors related to meteorological parameters and instrument noise but also systematic errors related to scattering by clouds and aerosols, which can dominate the error budget (Kawa et al., 2010; O'Dell et al., 2012). Furthermore, passive measurements have coverage gaps where there is insufficient sunlight and where there is excessive scattering.

In addition to the model transport examined by a number of inversion intercomparison studies (e.g. Gurney et al., 2002; Baker et al. 2006), the inversion technique and assumptions can contribute to substantial differences in results. For example, Chevallier et al. (2014) found that significant differences in hemispheric and regional flux estimates can stem from differences in Bayesian inversion techniques, transport models, a priori flux estimates, and satellite CO_2 retrievals. Houweling et al. (2015) presented an intercomparison of 8 different inversions using 5 independent GOSAT retrievals, and also found substantial differences in optimized fluxes at the regional level, with modeling differences (priors, transport, inversion technique) contributing approximately as much to the spread in results on land as the different satellite retrievals used.

105 In this paper, we present inversions of GOSAT and in situ data using a distinct technique,
106 which are compared with results from other studies. All of the previous GOSAT satellite data
107 inversions have used computationally-efficient approaches, such as variational and ensemble
108 Kalman filter data assimilation, to handle the large amounts of data generated by satellites and
109 the relatively large number of flux regions whose estimation is enabled by such data. The
110 computational efficiency of these approaches results from numerical approximations. In this
111 study, we apply a traditional, batch, Bayesian synthesis inversion approach (e.g. Baker et al.,
112 2006) at high spatiotemporal resolution relative to previous batch inversions to estimate global,
113 interannually varying CO_2 fluxes from satellite and in situ data. Advantages of this technique
114 include generation of an exact solution along with a full-rank error covariance matrix (e.g.
115 Chatterjee and Michalak, 2013), and an unlimited time window during which fluxes may
116 influence observations, unlike the limits typically imposed in Kalman filter techniques. The
117 major disadvantages of the batch technique are that computational requirements limit the
118 spatiotemporal resolution at which the inversion can be solved and the size of the data set that
119 can be ingested, a large number of transport model runs is required to pre-compute the basis
120 functions (i.e. Jacobian matrix), and the handling of the resulting volume of model output is very
121 time-consuming at relatively high resolution.
122 We estimate natural terrestrial and oceanic fluxes over the period May 2009 through
123 September 2010. The analysis spans two full boreal summers; longer periods were prohibited by
124 the computational effort. The objectives of this study are: 1) to understand recent variability of
125 the global carbon cycle, 2) to evaluate the bottom-up flux estimates used for the priors, 3) to
126 compare fluxes and uncertainties inferred using in situ observations, GOSAT observations, and
127 the two data sets combined and to assess the value added by the satellite data, and 4) to generate

inversion results using a unique Bayesian inversion technique for comparison with other approaches.

Section 2 provides details on the inputs and inversion methods. Section 3 presents prior and posterior model CO_2 mole fractions and their evaluation against independent data sets, fluxes and uncertainties at various spatial and temporal scales, and comparisons with results from inversions conducted by other groups. We discuss the robustness of results, and examine in particular their sensitivity to assumed prior flux uncertainties. We then analyze the possible impacts of several climatic events during the analysis period on CO_2 fluxes. Section 4 contains concluding remarks.

2. Methods

Our method is based on that used in the TransCom 3 (TC3) CO_2 inversion intercomparisons (Gurney et al., 2002; Baker et al. 2006) and that of Butler et al. (2010), the latter representing an advance over the TC3 method in that they accounted for interannual variations in transport and optimized fluxes at a higher spatial resolution. Our method involves further advances over that of Butler et al. (2010), including higher spatial and temporal resolution for the optimized fluxes, and the use of individual flask-air observations and daily averages for continuous observations rather than monthly averages. Inversion theoretical studies and intercomparisons have suggested that coarse resolution for flux optimization can produce biased estimates, i.e. estimates that suffer from aggregation error (Kaminski et al., 2001; Engelen et al., 2002; Gourdji et al., 2012). Although observation networks may not necessarily provide sufficient constraints on fluxes at high resolutions, Gourdji et al. (2012) adopted the approach of

151 estimating fluxes first at fine scales and then aggregating to better-constrained resolutions to
152 minimize aggregation errors. The high spatiotemporal resolution of our inversion relative to
153 other global batch inversions would be expected to reduce aggregation errors. Similarly, use of
154 higher temporal resolution observations allows our inversion to more precisely capture
155 variability due to transport and thus more accurately estimate fluxes. Details on our inversion
156 methodology are provided in the sub-sections below.
157
158 2.1. A priori fluxes and uncertainties
159 Prior estimates for net ecosystem production (NEP = photosynthesis − respiration) and
160 fire emissions (wildfires, biomass burning, and biofuel burning) come from the Carnegie-Ames-
161 Stanford-Approach (CASA) biogeochemical model coupled to version 3 of the Global Fire
162 Emissions Database (GFED3) (Randerson et al., 1996; van der Werf et al., 2006; 2010). CASA-
163 GFED is driven with data on fraction of absorbed photosynthetically active radiation (FPAR)
164 derived from the AVHRR satellite series (Pinzon et al, 2014; Los et al., 2000), burned area from
165 MODIS (Giglio et al, 2010), and meteorology (precipitation, temperature, and solar radiation)
166 from the Modern-Era Retrospective Analysis for Research and Applications (MERRA)
167 (Rienecker et al., 2011). CASA-GFED fluxes are generated at 0.5° x 0.5° resolution. For use in
168 the atmospheric transport model, monthly fluxes are downscaled to 3-hourly values using solar
169 radiation and temperature (Olsen and Randerson, 2004) along with MODIS 8-day satellite fire
170 detections (Giglio et al., 2006). In general, the biosphere is close to neutral in the CASA-GFED
171 simulation, i.e. there is no long-term net sink although there can be interannual variations in the
172 balance between uptake and release. In the version of CASA used here, a sink of ~100 Tg C y^{-1}
173 is induced by crop harvest in the U.S. Midwest that is prescribed based on National Agriculture

174 Statistics Service data on crop area and harvest. Although respiration of the harvested products
175 is neglected, the underestimate of emissions that is implied is geographically dispersed and in
176 principle correctable by the inversion.

177 For air-sea CO_2 exchange, monthly, climatological, measurement-based fluxes are taken
178 from Takahashi et al. (2009) for the reference year 2000 on a 4° x 5° lat/lon grid. In contrast to
179 the CASA-GFED flux being close to neutral on a global basis, the prior ocean flux forms a net
180 sink of 1.4 Pg C y^{-1}. (Note that the uncertainties we assign to the prior fluxes, discussed below,
181 are large enough to accommodate possible biases, e.g. the neutral biosphere rather than a sizable
182 net land sink as suggested by the literature.) For fossil CO_2, 1° x 1°, monthly- and interannually-
183 varying emissions are taken from the Carbon Dioxide Information Analysis Center (CDIAC)
184 inventory (Andres et al., 2012). This includes CO_2 from cement production but not international
185 shipping and aviation emissions. Oxidation of reduced carbon-containing gases from fossil fuels
186 in the atmosphere (~5% of the emissions; Nassar et al., 2010) is neglected, and the entire amount
187 of the emissions is released as CO_2 at the surface. Similarly, CO_2 from oxidation of biogenic and
188 biomass burning gases is neglected. The total amount of CO_2 chemical production from fossil-
189 fuel and biospheric gases is estimated to be ~1 Pg C y^{-1} (for year 2006; Nassar et al., 2010).

190 A priori flux uncertainties are derived from those assumed in the TC3 studies (Table 1),
191 rescaled to our smaller regions and shorter periods with the same approach as Feng et al. (2009).
192 A priori spatial and temporal error correlations are neglected in our standard inversions. The
193 neglect of a priori spatial error correlations is justified by the size of our flux optimization
194 regions, with dimensions on the order of one thousand to several thousand km, likely greater
195 than the error correlation lengths for our 2° × 2.5° grid-level fluxes. For example, Chevallier et

196 al. (2012) estimated a correlation e-folding length of ~500 km for a grid size close to ours of 300
197 km × 300 km based on comparison of a terrestrial ecosystem model with global flux tower data.
198
199 2.2. Observations and uncertainties
200 For constraining fluxes at relatively high temporal resolution, observations are chosen
201 that consist of discrete whole-air samples collected in glass flasks approximately weekly and
202 continuous in situ tall tower measurements of CO_2 mole fraction from the NOAA ESRL Carbon
203 Cycle Cooperative Global Air Sampling Network (Dlugokencky et al., 2013; Andrews et al.,
204 2009) supplemented with continuous ground-based measurements at 3 sites in East Asia from the
205 Japan Meteorological Agency (JMA) network (http://ds.data.jma.go.jp/gmd/wdcgg/cgi-
206 bin/wdcgg/catalogue.cgi, accessed 14 Mar 2013; Tsutsumi et al., 2006). Both data sets are
207 calibrated to the WMO-X2007 scale. In the present study, these data sets are referred to
208 collectively as "in situ" observations. The 87 sites (Fig. 1a) are chosen based on data availability
209 for the analysis period, Mar 2009-Sep 2010. Individual flask-air observations are used in the
210 inversions (with the average taken where there are multiple measurements at a particular hour—
211 up to two pairs of duplicate samples), and for the continuous measurements, afternoon averages
212 are used (between 1200 and 1700 local standard time), avoiding the difficulty of simulating the
213 effects of shallow nighttime boundary layers. For the towers, data from the highest level only is
214 used. We apply minimal filtering of the data. For the NOAA data sets, we exclude only the
215 flask samples or 30-second-average continuous data with "rejection" flags, retaining data with
216 "selection" flags (NOAA uses statistical filters and other information such as wind direction to
217 flag data that are likely valid but do not meet certain criteria such as being representative of well-
218 mixed, background conditions), since the reasonably high-resolution transport model used here

(Sect. 2.3) captures much of the variability in the observations beyond background levels. Furthermore, observations strongly influenced by local fluxes are typically assigned larger uncertainties by our scheme (described below), and therefore have less weight in the inversion. For the JMA data, we omit only the hourly data with flag = 0, meaning the number of samples is below a certain level, the standard deviation is high, and there is a large discrepancy with one or both adjacent hourly values. Although some of the observation sites used in our inversion are located close to each other, there is never any exact overlap in grid box (altitude and/or longitude-latitude) or in time. Thus, all of those sites are kept for the inversions, with observations at each site and day treated as independent (i.e. neglecting error correlations).

We estimate the uncertainties for the flask-air observations as the root sum square (RSS) of two uncertainty components: the standard deviation of the observations at a particular hour and a simple estimate of the model transport/representation error. For the first uncertainty component, we assign a value of 0.3 ppm if there is only one sample, and apply a minimum value of 0.01 ppm to avoid uncertainty values of 0. The transport/representation error estimation is similar to that of the NOAA CarbonTracker (CT) CO_2 data assimilation system (prior to the CT 2015 version) (Peters et al., 2007; http://carbontracker.noaa.gov), whereby a fixed "model-data mismatch" is assigned based on the type of site, e.g. marine, coastal, continental, or polluted, ranging from 0.4 ppm to 4 ppm. For the continuous measurements, we take the RSS of two uncertainty components: the afternoon root mean square (RMS) of the uncertainties of the 30-second or hourly average observations reported by the data providers (divided by the square root of the number of observations, N), and the standard error of all the 30-second/hourly mole fractions within an afternoon period. This represents an attempt to account for instrument error as well as transport/representation error. In addition, based on initial inversion results, we

enlarged all in situ total observation uncertainties by a factor of 2 to lower the normalized posterior cost function value (defined in Section 2.4) closer to 1 as appropriate for the chi-squared (χ^2) distribution (the final value of which is shown in Table 2). (Another test showed that further enlargement of the uncertainties to 3 times the original values, while lowering the cost function value further, does not substantially change the posterior fluxes overall.)

GOSAT measures reflected sunlight in a sun-synchronous orbit with a 3-day repeat cycle and a 10.5 km diameter footprint when in nadir mode (Yokota et al., 2009). The spacing between soundings is ~250 km along-track and ~160 km or ~260 km cross-track (for 5-point/3-point sampling before/after Aug 2010). We use the ACOS B3.4 near infrared (NIR) retrieval of column-average CO_2 dry air mole fraction (XCO_2), with data from June 2009 onward (O'Dell et al., 2012; Osterman et al., 2013). Filtered and bias-corrected land nadir, including high (H) gain and medium (M) gain, and ocean glint data are provided. Three truth metrics were used together to correct biases (separately for H gain, M gain, and ocean glint) (Osterman et al., 2013; Lindqvist et al., 2015; Kulawik et al., 2016): 1) an ensemble of transport model simulations optimized against in situ observations, 2) coincident ground-based column observations from the Total Carbon Column Observing Network (TCCON), which are calibrated to aircraft in situ profiles linked to the WMO scale (Wunch et al., 2011), and 3) the assumption that CO_2 mole fraction ought to exhibit little spatiotemporal variability in the Southern Hemisphere mid-latitudes, other than a seasonal cycle and long-term trend. For our inversions, we use the average of all GOSAT observations falling within a given 2° latitude × 2.5° longitude transport model column in a given hour. Figure 1b shows the frequency of the ACOS GOSAT observations across the model grid.

The values assumed for the GOSAT uncertainties are based in part on the retrieval uncertainties provided with the ACOS data set. Following guidance from the data providers, these are inflated by a factor of 2 over land and 1.25 over ocean for more realistic estimates of the uncertainties (C. O'Dell, pers. comm., 2013); Kulawik et al. (2016) recommended an overall scale factor of 1.9 for the similar ACOS B3.5 data set. In the case of multiple observations within a model grid, we estimate the overall uncertainty as the RMS of the uncertainties of the individual observations, divided by the square root of N. Error correlations between observations in different model grids and at different hours are neglected.

Inversions are conducted using different combinations of data, including the in situ data ("in situ-only"), the GOSAT data ("GOSAT-only"), and both ("in situ + GOSAT").

We use several additional data sets for independent evaluation of the inversion results. Aircraft measurements from the HIAPER Pole-to-Pole Observations (HIPPO) campaign consist of vertical profiles of climate-relevant gases and aerosols from the surface to as high as the lower stratosphere, spanning a wide range of latitudes mostly over the Pacific region (Wofsy et al., 2011). Five missions were conducted during different seasons in 2009-2011, with two of the missions overlapping with our analysis period. We use the "best available" CO_2 values derived from multiple measurement systems from the merged 10-second data product (Wofsy et al., 2012). Another data set, the 'Amazonica' aircraft measurements over the Amazon basin, is useful for evaluating inversion performance over tropical land. These measurements consist of profiles of several gases including CO_2 determined from flask samples from just above the forest canopy to 4.4 km altitude over 4 sites across the Brazilian Amazon starting in 2010, taken approximately biweekly (Gatti et al., 2014, 2016). Finally, the Japan-Russia Siberian Tall Tower Inland Observation Network (JR-STATION) of towers provides continuous in situ

measurements of CO_2 and CH_4 over different ecosystem types across Siberia beginning in 2002 (Sasakawa et al., 2010; Sasakawa et al., 2013). The JR-STATION data have been used in combination with other in situ observations in CO_2 flux inversions (Saeki et al., 2013b; Kim et al., 2017).

2.3. Atmospheric transport model and model sampling

We use the Parameterized Chemistry and Transport Model (PCTM) (Kawa et al., 2004), with meteorology from the NASA Global Modeling and Assimilation Office (GMAO) MERRA reanalysis (Rienecker et al., 2011). For this analysis, PCTM was run at a resolution of 2° latitude × 2.5° longitude and 56 hybrid terrain-following levels up to 0.4 hPa, and hourly temporal resolution. A "pressure fixer" scheme has been implemented to ensure tracer mass conservation, the lack of which can be a significant problem with assimilated winds (Kawa et al., 2004). Evaluation of PCTM over the years has shown it to a reliable tool for carbon cycle studies. For example, Kawa et al. (2004) showed that the SF_6 distribution from PCTM was consistent with that of observations and of the models in TransCom 2, suggesting that the interhemispheric and vertical transport were reasonable. PCTM performed well in boundary layer turbulent mixing compared to most of the other models in a TransCom investigation of the CO_2 diurnal cycle (Law et al., 2008). The TransCom-CH_4 intercomparison (Patra et al., 2011) showed that a more recent version of PCTM performed very well relative to observations in its interhemispheric gradients of SF_6, CH_3CCl_3, and CH_4 and interhemispheric exchange time, and follow-on studies (Saito et al., 2013; Belikov et al., 2013) demonstrated through evaluation against observed CH_4 and ^{222}Rn that the convective vertical mixing in PCTM was satisfactory overall.

Offshore prior terrestrial biospheric and fossil fluxes are redistributed to the nearest onshore grid cells in the model grid to counteract diffusion caused by our regridding the original fluxes to the coarser 2° x 2.5° resolution, as recommended in the TC3 protocol (Gurney et al., 2000).

The model is initialized with a concentration field appropriate for March 22, 2009 from a multi-year PCTM run with prior fluxes. The initial conditions are optimized in the inversions, as described in Sect. 2.4.

PCTM is sampled at grid cells containing in situ observation sites or GOSAT soundings, at the hours corresponding to the observations. To mimic the sampling protocol for coastal flask sites, which favors clean, onshore wind conditions, the model is sampled at the neighboring offshore grid cell if the cell containing the site is considered land according to a land/ocean mask. For in situ sites in general, an appropriate vertical level as well as horizontal location is selected. Specifically, the model CO_2 profile is interpolated to a level corresponding on average to the altitude above sea level of the observation site. This procedure is relevant primarily for mountain sites and tall towers as well as aircraft samples; the lowest model layer (with a thickness of ~100 m on average) was used for most other sites.

Model columns are weighted using ACOS column averaging kernels, as in the following (Eq. 15 from Connor et al., 2008):

$$\boldsymbol{X_{CO2}^{m}} = \boldsymbol{X_{CO2}^{a}} + \sum_{\mathrm{j}} \mathbf{h}_{\mathrm{j}} \mathbf{a}_{\mathbf{CO2,j}} (\mathbf{x}_{\boldsymbol{m}} - \mathbf{x}_{\boldsymbol{a}})_{\mathrm{j}}, \quad (1)$$

where $\boldsymbol{X_{CO2}^{m}}$ ($\boldsymbol{X_{CO2}^{a}}$) refers to the model (ACOS a priori) column average mole fraction, **h** is the pressure weighting function, $\mathbf{a_{CO2}}$ is the column averaging kernel, **x** refers to a CO_2 profile, and j is the level index.

Time series of model and observed mole fractions at selected flask and continuous sites spanning a range of latitudes, longitudes, elevations, and proximity to major fluxes are shown for the prior and for the in situ-only inversion in Fig. 2. The prior model as well as the in situ inversion captures much of the observed synoptic-scale variability. This suggests that the PCTM transport is reasonably accurate, consistent with the findings of Parazoo et al. (2008) and Law et al. (2008).

2.4. Inversion approach

The batch, Bayesian synthesis inversion approach optimizes in a single step the agreement between model and observed CO_2 mole fractions and between a priori and a posteriori flux estimates in a least-squares manner (e.g. Enting et al., 1995). As in the paper by Baker et al. (2006), the cost function minimized in this approach can be expressed as

$$J = (\mathbf{c}_{\text{obs}} - \mathbf{c}_{\text{fwd}} - \mathbf{Hx})^T \mathbf{R}^{-1} (\mathbf{c}_{\text{obs}} - \mathbf{c}_{\text{fwd}} - \mathbf{Hx}) + (\mathbf{x}_0 - \mathbf{x})^T \mathbf{P}_0^{-1} (\mathbf{x}_0 - \mathbf{x}), \quad (2)$$

where $\mathbf{c}_{\text{obs}} - \mathbf{c}_{\text{fwd}}$ are mismatches between the observations and the mole fractions produced by the prior fluxes, **H** is the Jacobian matrix relating model mole fractions at the observation locations to regional flux adjustments **x** (note that **x** is used differently here than in Eq. 1), **R** is the covariance matrix for the errors in $\mathbf{c}_{\text{obs}} - \mathbf{c}_{\text{fwd}}$, $\mathbf{x}_0$ is an a priori estimate of the flux

adjustments, and $\mathbf{P}_0$ is the covariance matrix for the errors in $\mathbf{x}_0$. The solution for the a posteriori flux adjustments, $\hat{\mathbf{x}}$, is

$$\hat{\mathbf{x}} = (\mathbf{H}^T\mathbf{R}^{-1}\mathbf{H} + \mathbf{P}_0^{-1})^{-1}(\mathbf{H}^T\mathbf{R}^{-1}(\mathbf{c}_{\text{obs}} - \mathbf{c}_{\text{fwd}}) + \mathbf{P}_0^{-1}\mathbf{x}_0), \quad (3)$$

and the a posteriori error covariance matrix is given by

$$\mathbf{P} = (\mathbf{H}^T\mathbf{R}^{-1}\mathbf{H} + \mathbf{P}_0^{-1})^{-1}. \quad (4)$$

Importantly, the posterior uncertainties do not account for possible biases, given that the Bayesian inversion framework adopted here, as in other CO_2 studies, assumes Gaussian error distributions with no bias (observation, transport, prior, etc.).

This study focuses on the variability of natural fluxes (terrestrial NEP and ocean), and thus considers adjustments to those fluxes only, assuming the prior estimates for the fossil and fire fluxes are correct. This is commonly done in CO_2 inversion studies (e.g. Gurney et al., 2002; Peters et al., 2007; Basu et al., 2013), with the rationale that the anthropogenic emissions are relatively well known, at least at the coarse spatial scales of most global inversions. In our inversion, flux adjustments are solved for at a resolution of 8 days and for each of 108 regions that are modified from the 144 regions of the Feng et al. (2009) inversion (Fig. 1a), which are in turn subdivided from the TC3 regions. (The choice of an 8-day flux interval is based on data considerations, e.g. the quasi-weekly frequency of the flask measurements and reasonable sampling by GOSAT.) This is a significantly higher resolution than the monthly intervals and 22/47 regions in the previous batch inversions of TC3/Butler et al. (2010), which allows us to

take advantage of the relatively high density of the GOSAT observations. One of our regions consists of low-flux areas (e.g. Greenland, Antarctica) as well as small offshore areas that contain non-zero terrestrial biospheric fluxes but do not fit into any of the TC3-based land regions, similar to what was done by Feng et al. (2009). We also created a region that includes areas with non-zero oceanic fluxes that do not fit into any of the TC3-based ocean regions according to our gridding scheme.

Grid-scale spatial patterns are imposed in our flux adjustments based on the natural fluxes, similar to TC3 and Butler et al. (2010), except that we use patterns specific to our prior NEP or air-sea flux averaged over each particular 8-day period, rather than annual mean net primary productivity (NPP) patterns over land and spatially constant patterns over the ocean. To ensure net changes in flux are possible across each region, absolute values are used for the flux patterns. Prior values of 0 are specified for all flux adjustments.

The initial conditions (i.c.) are also optimized at the same time as the fluxes via two parameters: a scale factor to the i.c. tracer (described below) that allows for overall adjustment of spatial gradients, and a globally uniform offset. A priori uncertainties of 0.01 for the scale factor and 30 ppm for the offset are prescribed. Inversion results from March 22 through April 30, 2009 are discarded to avoid the influence of any inaccuracies in the i.c. (Our tests showed that inferred fluxes after the first two months are insensitive to the treatment of i.c. For example, for an in situ inversion in which we did not allow adjustments in the i.c. and offset parameters, 8-day average flux results are very similar to those of the baseline inversion, especially after the first two months, with a mean correlation coefficient of 0.95 from June 2009 onward across all TC3 regions and a mean difference of 0.03 Pg C/yr.) Although the GOSAT data set begins in June 2009, the observations can provide some constraint on earlier fluxes.

For generating the prior mole fractions, $\mathbf{c}_{fwd}$, and constructing the Jacobian matrix, $\mathbf{H}$, transport model runs were performed for each of the prior flux types and an i.c. tracer, as well as a run with a flux pulse (normalized to 1 Pg C y^{-1}) for each of the 108 regions and 71 8-day periods. (The last period in 2009 is shortened to 5 days to fit cleanly within the year.) The i.c. tracer is initialized as described in Sect. 2.3 and transported without emissions or removals for the duration of the analysis period. Each flux pulse is transported for up to 13 months, after which the atmosphere is well mixed (within a range of 0.01 ppm). This procedure generated a massive amount of 3-D model output, ~30 terabytes (compressed). All of the model output was then sampled at the observation locations and times.

A singular value decomposition (SVD) approach is used instead of direct computation of Eq. 3 and Eq. 4 to obtain a stable inversion solution without any need for truncation of singular values below a certain threshold (Rayner et al., 1999). Use of the SVD technique is especially helpful in the case of the inversions using GOSAT data, since the Jacobian matrix is too large (92762 (102210) × 7674 for GOSAT (in situ + GOSAT)) to be successfully inverted on our system (with a single CPU).

3. Results

3.1. General evaluation of inversions, including short-term flux variability

Posterior model mole fractions are closer to the assimilated observations than are the prior mole fractions for the in situ-only, GOSAT-only, and in situ + GOSAT inversions, as desired, as suggested by Fig. 2 and indicated by the means and standard deviations of the model-observation differences over all observations shown in Fig. 3 (a, d, e, and f). Comparison of

421 posterior mole fractions with the data set not used (Fig. 3b, c), on the other hand, gives mean
422 differences not as close to 0 as in the comparison with the assimilated data (Fig. 3d and 3a,
423 respectively), and standard deviations that are larger than for the prior; this reflects the fact that
424 the in situ and GOSAT data sets are not necessarily consistent with each other and combine to
425 produce larger standard deviations than with the less variable prior model, which has not
426 assimilated any data. The improved agreement between model and assimilated observations is
427 reflected also in the cost function values before and after the inversions shown in Table 2. The
428 minimized cost function follows a χ^2 distribution, and should thus have a value close to 1
429 (normalized by the number of observations) for a satisfactory inversion (Tarantola, 1987; Rayner
430 et al., 1999). The posterior cost function values for all of the inversions are closer to 1 than the
431 prior values.
432 In addition to cross-evaluating the in situ-only and GOSAT-only inversions, we evaluate
433 both inversions against the independent, well-calibrated Amazon aircraft data set, which samples
434 an under-observed region with large, variable fluxes. Vertical profiles of the model and the
435 aircraft data (Fig. S1 in the supplementary material) show that the prior mole fractions often
436 exhibit a bias relative to the aircraft observations, especially in a boundary layer-like structure
437 below ~2 km altitude, with the sign of the average bias varying from season to season. The in
438 situ inversion exhibits worse agreement with the observations than the prior does more often than
439 it is better (e.g. with a root mean square error (RMSE) that is more than 1 ppm larger in 27 of 60
440 cases above 2 km and in 27 cases below 2 km, and more than 1 ppm smaller in only 12 cases
441 above 2 km and 14 cases below 2 km). The GOSAT inversion exhibits smaller discrepancies
442 with the observations than the in situ inversion does more often than the reverse, in both altitude
443 ranges. Furthermore, the GOSAT inversion is more often better than the prior than worse above

444 2 km. Overall statistics, computed separately for lower and higher altitudes, are shown in Fig. 4.
445 The model-observation histograms indicate that agreement with the aircraft observations is again
446 better for the GOSAT inversion than the in situ inversion, with smaller or comparable mean
447 differences and standard deviations. There is a near complete lack of in situ sites in the inversion
448 that are sensitive to Amazon fluxes (as suggested by Fig. 1a), contrasting with the availability of
449 some GOSAT data over the region (Fig. 1b), meaning that regional flux adjustments in the in situ
450 inversion are driven, often erroneously, by correlations with fluxes outside of the region (as will
451 be discussed in depth below in Sect. 3.3). The GOSAT inversion agrees with the aircraft
452 observations better than the prior does above 2 km, implying that incorporating GOSAT data in
453 the inversion results in better performance than no data. However, the posterior model-
454 observation differences have greater variance than the prior below 2 km. A possible explanation
455 for this is that the use of GOSAT observations in an inversion introduces more random error in
456 the model mole fractions; given that the GOSAT data are sparse over the Amazon, there is little
457 data averaging over the 8-day intervals and flux regions and random errors can thus have a
458 substantial impact. GOSAT errors presumably affect higher altitudes in the model less, since the
459 mole fractions there are influenced by fluxes across a broader area than at lower altitudes and
460 thus errors are averaged out to a greater extent.

461 Example time series of 8-day mean prior and posterior NEP and ocean fluxes for the in
462 situ-only and GOSAT-only inversions are shown in Fig. 5. Since the posterior fluxes in our
463 inversion regions tend to have large fractional (percentage) uncertainties, especially for the in
464 situ-only inversion, we focus in this paper on results aggregated to larger regions. To facilitate
465 comparison with other studies, results are aggregated to TC3 land and ocean regions, accounting
466 for error correlations. The posterior time series exhibit larger fluctuations than the prior time

series, especially for the in situ inversion over land. The fluctuations would presumably be smaller if we excluded flagged, outlier in situ observations or used a smoothed data product such as GLOBALVIEW-CO_2 (2009), which has been used in many inversions including those of TC3 and some of those in the Houweling et al. (2015) intercomparison. In addition, some of the fluctuations likely represent actual variability in the fluxes, while other fluctuations are probably noise. In fact, the calculated numbers of degrees of freedom for signal and noise (as defined by Rodgers, 2000) are 3525 and 4186 for the in situ inversion (summing up approximately to the number of inversion parameters, 7674) and 4925 and 2947 for the GOSAT inversion. This indicates that ~45% of the in situ inversion solution is based on actual information from the measurements, given the assumed prior and observation uncertainties, while ~65% of the GOSAT inversion solution is constrained by the measurements. The in situ data set is sparser than GOSAT, especially over land, and thus contains greater spatial sampling bias, so that many of the flux regions are under-determined and may exhibit so-called dipole behavior associated with negative error correlations (discussed further below).

Results for the in situ + GOSAT inversion (not shown in Fig. 5) lie mostly in between the in situ-only and GOSAT-only results. The fluxes generally lie closer to those of the GOSAT-only inversion for regions with a relatively low density of in situ measurements, including tropical and southern land regions, while they lie closer to those of the in situ-only inversion for regions with a relatively high density of in situ measurements, including northern land and many ocean regions. As expected, there are a larger number of degrees of freedom for signal, 6553, than for either the in situ-only or the GOSAT-only inversion (and fewer degrees of freedom for noise, 1632), indicating that the two data sets provide a certain amount of complementary information. Here, ~80% of the inversion solution is constrained by the measurements.

To average out noise in the posterior fluxes and to better observe the major features in the results, we show monthly average fluxes in Fig. 6. There is a similar onset of seasonal CO_2 drawdown in the GOSAT-only inversion and the CASA-GFED prior in Boreal North America, Temperate North America, and Boreal Asia, whereas the in situ-only inversion is noisier, similar to what was noted above. The GOSAT inversion suggests an overall shift in the global CO_2 sink from tropical and southern land to northern land regions relative to the prior and the in situ inversion, similar to what has been found in previous GOSAT inversions (e.g. Houweling et al., 2015; discussed further below). There are some unusual features in the GOSAT inversion. For example, there is a negative flux in January in some northern regions, with the 1σ range lying entirely below zero for Boreal Asia and Europe; this CO_2 uptake does not seem plausible in the middle of winter for these regions. Also, there are large positive fluxes during winter through spring in Northern Africa, which deviate from the prior beyond any overlap in the 1σ ranges for two months and whose 1σ ranges stay above zero for six months, summing up to a source of 1.9 Pg C over the period December through May, not including fires. The fluxes are larger than those of any sustained period of positive fluxes in any region in either the prior or the in situ inversion. The anomalous features suggest that the GOSAT inversion is affected by uncorrected retrieval biases that vary by season and region (as has been shown by Lindqvist et al. (2015) and Kulawik et al. (2016)) and/or sampling biases, including a lack of observations at high latitudes during winter, which limit the ability to accurately resolve inferred fluxes down to the scale of TransCom regions.

A comparison of the monthly mean fluxes with those from another inversion system, NOAA's CarbonTracker version 2013B (CT2013B), is displayed in Fig. 7. CT2013B is an ensemble Kalman smoother data assimilation system with a window length of five weeks that

513 uses multiple in situ observation networks and prior models to optimize weekly fluxes (Peters et
514 al., 2007; https://www.esrl.noaa.gov/gmd/ccgg/carbontracker/CT2013B/CT2013B_doc.php,
515 accessed 4 October 2016). Similar to the present study, CT2013B uses CASA-GFED3 fluxes
516 from van der Werf et al. (2010) as one of the land NEP priors, though with different FPAR and
517 meteorological driver data. (CASA-GFED2 is the other land prior in its ensemble of priors.) In
518 addition, CT2013B uses the seawater pCO_2 distribution from the Takahashi et al. (2009)
519 climatology to compute fluxes for one of its ocean priors; the other ocean prior is based on
520 results from an atmosphere-ocean inversion. CT2013B uses 93 observation time series while 87
521 are used here, although the former include measurements by multiple labs at the same site and
522 flask and continuous measurements at the same site (where duplicate observations are de-
523 weighted by inflating the model-data mismatch error by the square root of N). A notable
524 difference is that CT2013B solves for uniform flux scale factors over entire ecosystem types
525 within each TC3 region, with the ecosystem types not necessarily being contiguous. Results
526 from our in situ-only inversion are shown alongside those of CT2013B in Fig. 7 aggregated over
527 large regions. The two sets of posterior flux time series are similar overall, with overlapping 2σ
528 ranges at all times except in the extratropical northern oceans region. One distinctive feature is
529 that the posterior fluxes stay closer to the priors for CT2013B. A likely explanation is the tighter
530 prior uncertainties in CT2013B, the magnitudes of which are on average 40% of ours for land
531 regions and 30% of ours for ocean regions. For its ocean prior based on an atmosphere-ocean
532 inversion, CT2013B assumes uncertainties consistent with the formal *posterior* uncertainties
533 from the inversion, which are relatively small because of the large number of ocean observations
534 used in the inversion; uniform fractional uncertainties are assumed for the other ocean prior and
535 the land priors. Another feature is the larger month-to-month fluctuations in our results. In

addition to the tighter prior uncertainties used, another factor that could contribute to smaller fluctuations in the CT2013B results is the use of prior estimates that represent a smoothing over three assimilation time steps, which attenuates variations in the forecast of the flux parameters in time. And another factor is that to dampen spurious noise due to the approximation of the covariance matrix by a limited ensemble, CT2013B applies localization for observation sites outside of the marine boundary layer, in which flux parameters that have a non-significant relationship with a particular observation are excluded. We further evaluate our inversions in the following sections.

3.2. Longer-term budgets and observation biases

Longer-timescale budgets can be assessed in Fig. 8, which displays 12-month mean fluxes (Jun 2009-May 2010) over large, aggregated regions, with fires now included, for our inversions and the CT2013B inversion. Results for individual TC3 regions are shown in Table 1. The global total flux (including fossil emissions) is substantially more positive for the GOSAT-only inversion relative to the in situ-only inversion, 6.5 ± 0.2 Pg C y^{-1} vs. 4.1 ± 0.5 Pg C y^{-1}, while that for the in situ + GOSAT inversion lies in between at 5.7 ± 0.2 Pg C y^{-1}. Such a large difference in the atmospheric CO_2 growth rate implied by the two distinct data sets is plausible even if there are no trends in uncorrected biases between the data sets, given their sampling of different regions of the atmosphere and the relatively short 12-month time frame over which the growth occurs. In fact, for a different 12-month period within our analysis, Sep 2009-Aug 2010, the total fluxes for the GOSAT-only and in situ-only inversions are much closer to each other– 5.53 Pg C y^{-1} and 5.47 Pg C y^{-1}. Houweling et al. (2015) also found a larger total flux in the GOSAT-only inversions relative to the in situ during Jun 2009-May 2010 averaged across 8

559 models, ~4.8 Pg C y^{-1} vs. ~4.6 Pg C y^{-1}, with a substantial amount of inter-model variability
560 within those averages.

561 As was noted in Section 3.1, the GOSAT-only inversion exhibits a shift in the global CO_2
562 sink from tropical and southern land to northern land relative to the prior and the in situ-only
563 inversion (Fig. 8). The differences are within the 1σ uncertainty ranges. The shift includes an
564 increase in the source in N. Africa (0.2/1.5/2.0 Pg C y^{-1} for prior/in situ-only/GOSAT-only),
565 Temperate S. America (0.4/0.4/1.1 Pg C y^{-1}), and Australia (0.0/-0.2/0.6 Pg C y^{-1}), and an
566 increase in the sink in Europe (-0.1/0.6/-1.5 Pg C y^{-1}) and Temperate N. America (-0.3/-0.6/-1.5
567 Pg C y^{-1}) (Table 1). As for the ocean, the GOSAT inversion also exhibits a larger source in the
568 tropics relative to the prior and the in situ inversion (outside of the 1σ ranges; Fig. 8). However,
569 the GOSAT inversion now exhibits a smaller sink over extratropical northern oceans relative to
570 the in situ inversion, and a larger sink over extratropical southern oceans relative to both the
571 prior and the in situ inversion (at or outside of the 1σ ranges). The TC3 regions contributing the
572 most to these differences include Tropical Indian (0.1/0.0/0.7 Pg C y^{-1} for prior/in situ-
573 only/GOSAT-only), N. Pacific (-0.9/-0.5 Pg C y^{-1} for in situ-only/GOSAT-only), N. Atlantic (-
574 0.8/-0.5 Pg C y^{-1} for in situ-only/GOSAT-only), and Southern Ocean (-0.2/-0.4/-0.9 Pg C y^{-1} for
575 prior/in situ-only/GOSAT-only) (Table 1).

576 The GOSAT results appear to contradict global carbon cycle studies that favor a weaker
577 terrestrial net source in the tropics compensated by a weaker northern extratropical sink (e.g.
578 Stephens et al., 2007; Schimel et al., 2015). We show the north-south land carbon flux
579 partitioning of our results in Fig. S2 in the manner of Schimel et al. (2015). The shift in the sink
580 from the south + tropics to the north in the GOSAT inversion relative to the in situ inversion
581 goes in a direction opposite to that consistent with an airborne constraint considered by Stephens

et al. (2007) and with the expected effect of CO_2 fertilization according to Schimel et al. (2015). However, the shift may be due at least in part to GOSAT retrieval and sampling biases. An evaluation of posterior mole fractions in the GOSAT-only inversion against surface in situ observations indicates that the GOSAT inversion may be biased low during much of the analysis period over Europe and Temperate N. America, especially in winter (when there is little direct constraint at high latitudes by GOSAT observations), and biased somewhat high over N. Africa, especially in spring. However, the dearth of in situ sites over N. Africa, with only one in the middle of the region (in Algeria) and a few around the edges (e.g. Canary Islands and Kenya), precludes a definitive evaluation over that region. Globally, the GOSAT inversion tends to underestimate mole fractions at high latitudes of the Northern Hemisphere, often by more than 1σ, as shown by latitudinal profiles averaged over all surface sites by season (Fig. 9), suggesting an overestimated northern sink. The same is true of the high latitudes of the Southern Hemisphere. The GOSAT inversion overestimates mole fractions in parts of the tropics, sometimes by more than 1σ (Fig. 9), suggesting an overestimated tropical source. Uncorrected retrieval biases may be especially prevalent in the tropics, where there are very few TCCON stations available as input to the GOSAT bias correction formulas; only 1 TCCON station, Darwin, Australia, was operating in the tropics during 2009-2010, and only 2 more stations, Reunion Island and Ascension Island, became operational during the rest of the ACOS B3.4 retrieval period. In contrast, the posterior mole fractions for the in situ-only inversion generally agree well with the surface observations (Fig. 9; also seen in the individual site time series in Fig. 2), which is expected given that these are the observations that are used in the optimization. The prior mole fractions are generally too high, which is consistent with the fact that the CASA-

GFED biosphere is near neutral while the actual terrestrial biosphere is thought to generally be a net CO_2 sink.

Evaluation of the inversions against latitudinal profiles constructed from HIPPO aircraft measurements, which provide additional sampling over the Pacific, does not indicate any widespread overestimate by the GOSAT inversion relative to the observations in the tropics (Fig. 10a-f), unlike what was seen in the comparison with the more globally distributed surface observations. But the GOSAT inversion does exhibit an underestimate relative to HIPPO from ~40°S southward in the lower to middle levels of the troposphere (Fig. 10a, b, d, e), especially for Mission 2 (Oct-Nov 2009). Again, retrieval bias and sampling bias (a lack of GOSAT ocean observations south of ~40°S and land observations south of ~50°S) are likely the causes of the underestimate. In the northern extratropics, the GOSAT inversion actually exhibits higher mean mixing ratios than HIPPO in general in the lower troposphere, especially for Mission 2, and the in situ inversion gives higher mixing ratios than HIPPO at some latitudes and lower mixing ratios at others for Mission 2. In one particular latitude range, 55-67°N, both inversions give much higher mixing ratios than HIPPO, by up to 67 ppm in the case of the in situ inversion and 30 ppm for the GOSAT inversion. This could reflect inaccuracy in posterior fluxes due to the inversions' being under-constrained over the high-latitude North Pacific and Alaska, with few observations during this season in the case of GOSAT and a tendency for the sparse in situ network to produce noisy inversion results, as was discussed above. However, given that the prior model also gives substantially higher mixing ratios than HIPPO at these latitudes (by up to 11 ppm), the discrepancy could be due in part to some factor common to the prior and posteriors such as model transport or representation error.

In the upper troposphere to lower stratosphere, the GOSAT inversion more often than not exhibits better agreement with the HIPPO observations than the in situ inversion does for both Mission 2 and 3 (Fig. 10c, f). (We think it is reasonable to include data from these altitudes as part of the evaluation of the inversion results, since the tropopause in the GEOS-5/MERRA meteorological data assimilation system underlying PCTM transport is considered to be accurate (Wargan et al., 2015) and PCTM has been shown to simulate upper troposphere-lower stratosphere trace gas gradients well compared to other models (Patra et al., 2011).) A likely explanation is that the GOSAT data provide constraints throughout the atmospheric column, whereas the in situ measurements constrain only surface CO_2. Figure 10 shows that the high-altitude mole fractions from the in situ inversion are consistently close to those of the prior, suggesting that the lack of high-altitude constraints prevents major adjustments in mole fractions at these levels, unlike in the GOSAT inversion. Regarding potential impacts of GOSAT biases, an air parcel at higher altitudes, especially in the upper troposphere or above, generally consists of a mixture of air originating from a broad area near the surface (e.g. Orbe et al., 2013), and thus the effects of different regional biases in posterior fluxes may cancel out at those altitudes.

The conclusion that GOSAT biases may contribute to the shift in the land sink is also supported by Houweling et al. (2015). That study reported a shift in the GOSAT-only inversions relative to the in situ inversions consisting of an increase in the sink in northern extratropical land of 1.0 Pg C y^{-1} averaged across models and an increase in the source in tropical land of 1.2 Pg C y^{-1} during June 2009-May 2010; in comparison, our inversions produce an increase in the northern land sink of 0.4 Pg C y^{-1} and an increase in the tropical land source of 1.2 Pg C y^{-1} (Fig. 8). Houweling et al. (2015) found an especially large and systematic shift in flux of ~0.8 Pg C y^{-1} between N. Africa and Europe, but then provided evidence that the associated latitudinal

649 gradient in CO_2 mole fractions may be inconsistent with that based on surface and HIPPO
650 aircraft in situ observations. They also suggested that the shift in annual flux between the two
651 regions may be a consequence of sampling bias, with a lack of GOSAT observations at high
652 latitudes during winter. Chevallier et al. (2014) also found a large source in N. Africa of ~1 Pg C
653 y^{-1} in their ensemble of GOSAT inversions and considered the magnitude of that unrealistic,
654 given that emissions from fires in that region likely amount to < 0.7 Pg C y^{-1}. (Note that our N.
655 Africa source is even larger than that of Chevallier et al. (2014).) Inversion experiments by Feng
656 et al. (2016) provide evidence that the large European sink inferred from GOSAT observations
657 may be an artifact of high XCO_2 biases outside of the region that necessitate extra removal of
658 CO_2 from incoming air for mass balance, in concert with sub-ppm low XCO_2 biases inside the
659 region. An observing system simulation experiment by Liu et al. (2014) found that GOSAT
660 seasonal and diurnal sampling biases alone could result in an overestimated annual sink in
661 northern high-latitude land regions. And a review paper by Reuter et al. (2017) further
662 highlighted the discrepancy between satellite-based and ground-based estimates of European
663 CO_2 uptake and cited retrieval and sampling biases as possible sources of error in the former
664 (while also noting sampling issues with in situ networks for the region).

665 Again, the results for the in situ + GOSAT inversion lie mostly in between those for the
666 in situ-only and GOSAT-only inversions, with the in situ + GOSAT fluxes lying closer to the
667 GOSAT-only ones for the tropical/southern land regions and land as a whole (Table 1 and Fig.
668 8), suggesting the dominance of the GOSAT constraint in these regions. The posterior
669 uncertainties for the GOSAT inversion (Table 1) are as small as or smaller than those for the in
670 situ inversion, except in Boreal and Temperate N. America, N. Pacific, Northern Ocean, and
671 Southern Ocean. This reflects the fact that GOSAT generally provides better spatial coverage,

except over N. America, where the in situ network provides good coverage, and over and near high-latitude ocean areas, where there is decent in situ coverage and poor GOSAT coverage. Uncertainty reductions in the in situ inversion range from 15% to 93% for land regions and 15% to 56% for ocean regions (Table 1). In the GOSAT inversion, the uncertainty reductions range from 43% to 89% for land and 19% to 56% for ocean. And in the inversion with combined in situ and GOSAT data, the uncertainty reductions are larger than or equal to those in either the in situ-only or the GOSAT-only inversion, ranging from 61% to 96% for land and 40% to 67% for ocean.

3.3. Flux error correlations and land-ocean partitioning

Here we elaborate on posterior error correlations, which indicate the degree to which fluxes are estimated independently of one another. Negative correlations can be manifested in dipole behavior, in which unusually large flux adjustments of opposite signs occur in neighboring regions/time intervals. These are shown in Fig. 11 aggregated to TC3 regions and the 12-month period from June 2009 to May 2010. The full-rank error covariance matrix generated by the exact Bayesian inversion method (from which the correlation coefficients are derived) is a unique product of this study, particularly as applied to satellite data. There are a larger number of sizable correlations between land regions in the in situ inversion than in the GOSAT inversion (in the top left quadrants of the plots). One specific feature is negative correlations among the four TC3 regions in South America and Africa ("Trop Am", "Temp S Am", "N Africa", and "S Africa") in the in situ inversion, whereas in the GOSAT inversion there are negative correlations within South America and within Africa but not between the two continents. Although there are less extensive correlations over land in the GOSAT inversion,

695 they are often of larger magnitude than in the in situ inversion; this could reflect the fact that
696 GOSAT observations, though of higher density than the in situ observations over many regions,
697 are column averages representing mixtures of air from a broader source region than for surface
698 observations, and may thus result in larger error correlations for immediately adjacent regions,
699 e.g. within a continent. Over the ocean regions, in contrast, the GOSAT inversion exhibits anti-
700 correlations that are as extensive as those for the in situ inversion and often of larger magnitude.
701 For example, there are substantial negative correlations between Southern Ocean and each of the
702 other southern regions—S. Pacific, S. Atlantic, and S. Indian. This is consistent with the almost
703 complete lack of GOSAT observations at the latitudes of the Southern Ocean region and the
704 southern edges of the neighboring ocean regions (Fig. 1b). Interestingly, there is not a sizable
705 correlation between N. Africa and Europe in the GOSAT inversion (in either seasonal or 12-
706 month means), which runs counter to what might be expected from the shift in flux discussed
707 above; rather, each of these regions is correlated with a number of other regions. We do find a
708 fairly large correlation of -0.62 between the northern extratropics in aggregate (land + ocean) and
709 the tropics for the 12-month period though. Correlations for the in situ + GOSAT inversion (not
710 shown) generally lie in between those of the in situ-only and GOSAT-only inversions. Even
711 with the incorporation of both sets of observations, there are substantial correlations of as much
712 as -0.6 between regions within a continent, reinforcing our earlier conclusion that sampling gaps
713 limit the ability of the observations to constrain fluxes down to the scale of most TC3 regions.
714 The in situ-only and CT2013B posterior global totals are nearly the same, but the land-
715 ocean split is different, with our inversion exhibiting a larger sink over ocean than over land
716 (with non-overlapping 2σ ranges) while in CT2013B the land and ocean fluxes are similar, with
717 the ocean flux changing little from the prior (Fig. 8). A likely explanation for the difference is

718 the very tight prior constraints on ocean fluxes of CT2013B that were discussed above, which
719 force the flux adjustments to take place mostly on land. The GOSAT inversion also exhibits a
720 relatively large ocean sink of -3.1 ± 0.5 Pg C y^{-1}; for comparison, the CT2013B estimate is -2.4 ±
721 0.4 Pg C y^{-1}, our in situ-only estimate is -4.0 ± 0.8 Pg C y^{-1}, and the estimate of the Global
722 Carbon Project (GCP) is -2.5 ± 0.5 Pg C y^{-1} for 2009-2010 (Le Quéré et al., 2013; Le Quéré et
723 al., 2015). The GCP estimate is a synthesis that combines indirect observation-based estimates
724 for the mean over the 1990s with interannual variability from a set of ocean models and accounts
725 for additional observation-based estimates in the uncertainty. The difference between our
726 inversion estimates and the GCP estimate is actually even larger than suggested by those
727 numbers, given that a background river to ocean flux of ~0.5 Pg C y^{-1} should be subtracted from
728 our ocean flux to make it comparable to the GCP ocean sink, which refers to net uptake of
729 *anthropogenic* CO_2 (Le Quéré et al., 2015). Our relatively small land sink is reflected in our
730 inversion results' lying mostly outside of the GCP global land flux range in the north-south
731 partitioning plot in Fig. S2. Similarly, in comparing our results with those of Houweling et al.
732 (2015), we find that the global budgets are comparable for all three inversions—in situ-only,
733 GOSAT-only, and in situ + GOSAT—as was mentioned above, but the land-ocean split is
734 different. Our posterior ocean flux is -4.0 ± 0.8 Pg C y^{-1}, -3.1 ± 0.5 Pg C y^{-1}, and -3.9 ± 0.3 Pg C
735 y^{-1} for the three inversions, while it is -1.6 ± 0.5 Pg C y^{-1}, -1.2 ± 0.6 Pg C y^{-1}, and -1.5 ± 0.8 Pg C
736 y^{-1} in the results of Houweling et al. (2015; pers. comm., 2016) (averaged over different
737 weighted averages of the models).

738 There is a strong negative correlation globally between posterior flux errors for land and
739 ocean of -0.84 and -0.89 in the in situ-only and the GOSAT-only inversion, respectively. Basu et
740 al. (2013) also reported a large negative correlation between land and ocean fluxes of -0.97 in

741 their in situ + GOSAT inversion during September 2009-August 2010. The anti-correlations
742 imply that the observations cannot adequately distinguish between adjustments in the global land
743 and ocean sinks. Thus, land-ocean error correlation may be a fundamental challenge that global
744 CO_2 flux inversions are faced with, at least given the sampling characteristics of the in situ and
745 GOSAT data sets used here. Without tight prior constraints on ocean fluxes, those fluxes are
746 subject to large, and potentially unrealistic, adjustments (i.e. dipole behavior).
747 To assess the effect of prior constraints on the inversion, we conducted a test with
748 reduced prior uncertainties, for both land and ocean fluxes, so that they are similar on average to
749 those of CT2013B. Results for an in situ-only inversion and a GOSAT-only inversion are shown
750 in Table 1 and Fig. 12. For the in situ-only inversion, the posterior ocean flux is now much
751 smaller in magnitude, -2.8 ± 0.3 Pg C y^{-1}. The posterior ocean flux for the GOSAT inversion
752 does not change as much, decreasing in magnitude from the original -3.1 ± 0.5 Pg C y^{-1} to $-2.9 \pm$
753 0.2 Pg C y^{-1}. The ocean flux 1σ ranges for both inversions now overlap with the 1σ range of
754 CT2013B; accounting for the riverine flux, the 1σ range for the in situ inversion overlaps with
755 the 1σ range of GCP, while the 1σ range for the GOSAT inversion is still just outside of that of
756 GCP. The better agreement with the GCP budget (land component) can also be seen in Fig. S2
757 for both inversions. The inversions with tighter priors have slightly larger cost function values
758 than the baseline inversions (Table 2; the difference for the GOSAT cases is concealed by
759 rounding). The inversions with tighter priors generally exhibit better agreement with
760 independent observations, e.g. lower-altitude HIPPO observations (Fig. S3), and surface
761 observations in the case of the GOSAT inversion (Fig. S4), indicating that the effects of
762 sampling and retrieval biases are reduced with tighter prior uncertainties. The better agreement
763 also lends support to the smaller ocean sink estimates. (At high altitudes, keeping posterior mole

764 fractions closer to the prior mole fractions results in worse agreement with HIPPO in many
765 places, especially for the GOSAT inversion.) However, the tighter priors do not completely
766 eliminate the discrepancies between the inversions and the independent observations, suggesting
767 that tight priors may not completely counteract the effects of observational biases.

768 Basu et al. (2013) saw a similar underestimate of mole fractions during parts of the year
769 in the southern extratropics in their GOSAT inversion relative to surface observations and
770 overestimate of the seasonal cycle, though with some differences in the shape of the seasonal
771 cycle from our study (including a later descent toward and recovery from the annual minimum in
772 austral summer and a larger peak in late winter-early spring). They, however, used the SRON-
773 KIT RemoTeC GOSAT retrieval with a known issue over the ocean, and concluded that adding
774 global land and ocean observation bias correction terms to their inversion was needed to make
775 the land-ocean flux split more realistic and to improve the seasonal cycle of CO_2 in the southern
776 extratropics. In contrast, studies have found no noticeable bias in the ACOS B3.5 ocean glint
777 XCO_2 retrievals relative to TCCON (Kulawik et al., 2016) and a mean bias of only -0.06 ppm
778 relative to HIPPO (Frankenberg et al., 2016); the B3.4 version we use is on average ~0.2 ppm
779 lower than B3.5 in 2010 (Deng et al., 2016). So although a small overall negative bias in the
780 bias-corrected ACOS B3.4 ocean data cannot be ruled out (and there could of course be larger
781 negative biases on a regional scale, such as in the southern extratropics), we conclude that the
782 land-ocean flux split in inversions using either in situ or GOSAT data is strongly influenced by
783 error correlations and dependent on the prior uncertainties assumed.

784 The shift in the global terrestrial sink from the tropics/south to the north when comparing
785 the GOSAT-only inversion with the in situ-only inversion and the prior is still seen when prior
786 uncertainties are decreased (Fig. 12; Fig. S2), as is a substantially more positive global total

787 budget in the GOSAT inversion relative to the in situ (Fig. 12). The uncertainty reductions in the
788 test inversions are smaller than those in the baseline inversions (Table 1), as is expected from the
789 smaller starting values of the uncertainties. In summary, the magnitude of the ocean sink and the
790 partitioning of the global sink between land and ocean are sensitive to the prior uncertainties, but
791 other inferred features of the carbon budget are robust with respect to prior uncertainties.
792 Given that there is uncertainty in the land-ocean flux partitioning at sub-global scales as
793 well (e.g. as indicated by moderate negative correlations between northern land and northern
794 oceans, tropical land and tropical oceans, etc.), we consider results for combined land and ocean
795 regions in Figs. 8 and 12. They indicate that there is a shift in the global sink from the tropics to
796 the north and the south in the GOSAT inversion relative to the prior, and an increased source in
797 the tropics of ~2 Pg C y^{-1} in the GOSAT inversion relative to the in situ inversion. These
798 features are seen in the inversions with tighter priors as well as in the baseline inversions. Note
799 that the increased source over southern land and increased sink over southern oceans in the
800 GOSAT inversion relative to the in situ inversion that were discussed earlier cancel each other
801 out approximately, suggesting a compensation of errors. Also note that the inversion using the in
802 situ + GOSAT data sets, which provide more constraint than either of the data sets alone,
803 produces a global flux close to mid-way between the in situ-only and GOSAT-only inversions,
804 while it produces a Tropic Land + Oceans flux much closer to that of the GOSAT inversion than
805 to the in situ inversion. This suggests some degree of independence of the GOSAT-inferred
806 regional result from the global result.
807
808 3.4. Impacts of climatic conditions on 2009-2010 fluxes

809 We now analyze the impacts of several climatic events during the analysis period on CO_2
810 fluxes as indicated by the inversion results. We focus on 1) unusually hot and dry conditions at
811 Northern Hemisphere higher latitudes in summer of 2010, 2) wetter conditions over parts of
812 North America in spring and early summer of 2010 relative to 2009, and 3) record drought in the
813 Amazon in 2010.
814 Guerlet et al. (2013), who examined GOSAT data and performed a flux inversion using a
815 variational assimilation system, found that there was less net terrestrial CO_2 uptake in summer of
816 2010 than in 2009 at northern high latitudes, consistent with known severe heat waves, drought,
817 and high fire emissions, especially across Eurasia, centered around western Russia, and to a
818 lesser extent in North America.
819 Motivated by that study, we examined our inversion results for 2009 and 2010, focusing
820 on the GOSAT inversion. As can be seen in the global maps of natural plus biomass burning
821 fluxes in June-July-August (JJA) in Fig. 13, the GOSAT inversion does appear to exhibit a
822 decreased CO_2 uptake over Eurasia, including the area around western Russia (enclosed in a box
823 in the figure), in 2010. A decreased sink can also be seen in parts of North America. A
824 decreased sink over western Russia can also be seen in the CASA-GFED prior, though of a
825 smaller magnitude. In contrast, there is actually an increased sink in that region in the in situ
826 inversion. In fact, none of the sites used are in or immediately downwind of that region (Fig.
827 1a). Total NEP and fire fluxes over northern TC3 regions are shown in Fig. 14. There is less
828 CO_2 uptake in JJA 2010 than in 2009 in all the regions except Temperate Asia in the GOSAT-
829 only inversion. The differences exceed the 1σ ranges for 3 of the 5 regions, even exceeding the
830 3σ ranges for Europe, which includes western Russia. Also shown is the in situ + GOSAT
831 inversion, which exhibits a similar pattern of 2010-2009 differences. These inversion results are

thus consistent with the earlier GOSAT study. In contrast, the 2010-2009 differences in the prior are small and, for some regions, of the opposite sign as that in the inversions (Fig. 14).

Measurements from the JR-STATION tower network are suitably located for evaluating the inferred flux interannual variability over Eurasia. Time series are shown in Fig. 15 for observations, the prior model, and the GOSAT-only inversion at 6 sites with complete summertime data in 2009-2010. (As with the continuous measurements used in the in situ inversion, afternoon data are selected to avoid difficulties associated with nighttime boundary layers.) Posterior mole fractions are noisier in the wintertime, likely a result of the lack of GOSAT observations during that season at these high latitudes. Focusing on 2010-2009 differences, the observations suggest a shallower drawdown in 2010 than in 2009 at most of the sites, which is generally captured by both the prior and the GOSAT posterior. It appears though that the GOSAT inversion exaggerates the 2010-2009 difference at some of the sites, overestimating especially the drawdown in 2009. For a more quantitative analysis, we calculate the average 2010-2009 difference in mole fractions over June-July-August for each site (Table 3). The GOSAT-only inversion overestimates the 2010-2009 difference at 5 of the 6 sites. The in situ + GOSAT inversion exhibits less of an overestimate overall than the GOSAT-only inversion, with 3 of the 6 sites being substantially overestimated. The prior exhibits the best agreement with the observations overall.

The earlier study by Guerlet et al. (2013) assumed that the differences between 2010 and 2009 posterior biospheric fluxes are relatively insensitive to biases in the GOSAT data, since at least some of those errors may be similar between the two years. However, our evaluation of the inversions using JR-STATION data suggests that retrieval biases can vary significantly from year to year. Kulawik et al. (2016) estimated a year-to-year variability in GOSAT biases relative

855 to TCCON of 0.3 ppm averaged over the stations. Another study has raised a separate but
856 related issue of inversion results potentially being sensitive to the spatiotemporal distribution of
857 observations in different data sets (e.g. different GOSAT retrievals) (H. Takagi, pers. comm.,
858 2015); by extension, comparison of fluxes from two time periods can be affected by changes in
859 the distribution of observations over time within a particular data set. But in JJA 2009 and 2010,
860 there are similar numbers of ACOS GOSAT observations overall in the northern land region, so
861 differences in data coverage are probably not a factor in this particular case study.

862 Our evaluation using JR-STATION data also indicates that the prior may be a reasonable
863 estimate of the 2010-2009 difference in growing season fluxes, at least over Siberia, despite
864 possible shortcomings in the simulation of drought impacts on NEP and of the overall magnitude
865 of fire emissions by CASA-GFED3. The latest version of GFED (version 4s), which includes
866 small fires, tends to generate higher emissions than GFED3 (van der Werf et al., 2017).

867 Over large parts of North America, conditions were wetter in spring and early summer of
868 2010 than in 2009, especially in the western half of the U.S. and adjacent parts of Mexico and
869 Canada, as suggested by North American drought maps for June 2010 vs. June 2009 (e.g.
870 https://www.drought.gov/nadm/content/map/2010/06) and shallow groundwater status maps for
871 the U.S. based on GRACE (Gravity Recovery and Climate Experiment) satellite data for May-
872 June (Houborg et al., 2012; http://droughtcenter.unl.edu/NASA/GRACE/). Consistent with the
873 wetter conditions in 2010 are a larger CO_2 sink over North America (Boreal + Temperate) in
874 May-June 2010 relative to 2009 in our priors (-5.0 ± 3.9 Pg C y^{-1} vs. -3.4 ± 3.9 Pg C y^{-1}), in situ-
875 only posteriors (-5.0 ± 0.4 Pg C y^{-1} vs. -3.8 ± 0.5 Pg C y^{-1}), and GOSAT-only posteriors ($-5.8 \pm$
876 0.4 Pg C y^{-1} vs. -3.3 ± 1.8 Pg C y^{-1}). We consider the in situ inversion result to be reliable here,
877 given the large uncertainty reduction for North America and small error correlations with other

878 regions (not shown). The 2010 and 2009 fluxes differ such that their 1σ ranges do not overlap
879 for the in situ and the GOSAT posteriors. Much warmer conditions in eastern North America in
880 May-June 2010 compared to 2009 (e.g. https://www.ncdc.noaa.gov/sotc/global/201005 and
881 https://www.ncdc.noaa.gov/sotc/global/200905) may have also contributed to increased uptake,
882 especially at higher latitudes, where insufficient warmth can be more of a limiting factor for NEP
883 than insufficient moisture during late spring-early summer. Despite the increased sink in June
884 2010 over North America, the 2010 summer exhibits a decreased sink relative to 2009 when
885 integrated through JJA (Fig. 14).

886 The Amazon basin experienced a record drought in 2010, which led to decreased
887 vegetation greenness and a net carbon loss to the atmosphere (Xu et al., 2011; Gatti et al., 2014).
888 Dry conditions in the north and center of the basin in the first three months were caused by the El
889 Niño of late 2009-early 2010, and an enhanced and prolonged dry season in the southern areas of
890 the basin was connected to an Atlantic sea surface temperature anomaly during the second half
891 of the year (Gatti et al., 2014). According to our prior estimate, fire emissions minus NEP
892 represented a near-zero net flux of -0.1 ± 2.1 Pg C y^{-1} in Jul-Sep 2010 (a period that includes
893 peak drought conditions and fire counts of that year) and a sink of -1.9 ± 2.1 Pg C y^{-1} in Jul-Sep
894 2009 in the TC3 Tropical America region. (The fire emissions amounted to 2.0 Pg C y^{-1} and 0.2
895 Pg C y^{-1} in Jul-Sep 2010 and 2009, respectively, while NEP was 2.1 Pg C y^{-1} in both periods.)
896 However, our GOSAT inversion suggests the reverse, -0.9 ± 0.6 Pg C y^{-1} vs. -0.4 ± 0.3 Pg C y^{-1}
897 for Jul-Sep 2010 and 2009, respectively. (We do not report the analogous results for the in situ
898 inversion, since the uncertainties are large in this undersampled region.) The prior estimate
899 seems more consistent with the expected impact of drought on fluxes than the inversion estimate
900 does. The inversion is hampered in the region by the relatively small number of GOSAT

soundings that are retrieved and pass the quality filters, especially during the burning season (with substantial light scattering by aerosols) and the rainy season (with extensive cloud cover). The dearth of observations results in relatively large posterior uncertainties and/or sizable flux error correlations. Furthermore, there is differing data coverage, with 2010 having fewer observations than 2009 in the TC3 Tropical America region during the height of the fire season (85 and 20 in Aug and Sep 2010 vs. 101 and 33 in 2009) and more observations than 2009 in July (150 vs. 85). The differing data coverage itself could affect the flux estimates differently in 2009 and 2010. The Amazonica data set does not enable an evaluation of the flux estimates for both 2009 and 2010, since the data set begins in 2010. However, comparison of the prior and GOSAT model mole fractions in 2010 with the Amazonica data shows that biases for both can vary substantially over time, e.g. in July vs. Aug-Sep (Fig. S1). This raises the possibility that neither the prior nor the GOSAT inversion correctly estimates the interannual flux difference in this region and also supports the idea that inversion bias can vary with data coverage.

4. Discussion and conclusions

We have successfully applied a global, high-resolution, batch Bayesian CO_2 inversion method to surface in situ observations and passive satellite column measurements from GOSAT and compared the flux estimates with ones using Kalman filter and variational approaches that involve various approximations. The exact inversion method provides full posterior error covariances, which allows us to quantitatively evaluate the degree to which regional fluxes are constrained independently of one another. However, for inversions over longer periods, using

923 larger volumes of data such as from OCO-2, or at higher flux resolution, more computationally
924 efficient methods are essential.

925 The GOSAT inversion is generally better constrained than the in situ inversion, with
926 smaller posterior regional flux uncertainties and correlations, except in places like North
927 America and northern and southern high-latitude ocean where the in situ observation networks
928 used provide relatively good coverage. Note that our in situ inversion did not make use of all the
929 surface monitoring sites that operated during the analysis period, omitting for example a number
930 of sites operated exclusively by agencies in Canada, Australia, and Europe
931 (http://ds.data.jma.go.jp/gmd/wdcgg/cgi-bin/wdcgg/catalogue.cgi), and that the surface networks
932 have been enhanced with additional sites since then. Furthermore, the in situ data sets that we
933 used for evaluation of the inversions, including JR-STATION and Amazonica, could also be
934 used as input in the inversions. And yet other aircraft data sets such as CONTRAIL, which
935 samples large parts of the Pacific and some other areas (Niwa et al., 2012), and NOAA's regular
936 aircraft profiles over mostly North America
937 (https://www.esrl.noaa.gov/gmd/ccgg/aircraft/index.html) and column measurements such as
938 from TCCON could be added. The use of GOSAT data in combination with in situ data provides
939 even greater flux uncertainty reductions than the use of either data set alone, indicative of
940 complementary constraints in the two datasets. Nevertheless, remaining coverage gaps,
941 including a lack of GOSAT observations at high latitudes during winter over land and year-round
942 over the ocean, and spatially, seasonally, and interannually varying coverage over tropical land,
943 limit the ability to accurately resolve fluxes down to the scale of TransCom sub-continental/sub-
944 ocean basin regions.

945 Our GOSAT inversion suggests a shift in the global terrestrial CO_2 sink from the tropics
946 and south to the north, relative to the prior and the in situ inversion; for combined land and ocean
947 fluxes, the GOSAT inversion produces a shift in the global sink from the tropics to the north and
948 the south relative to the prior, and an increased source in the tropics of ~2 Pg C y^{-1} relative to the
949 in situ inversion. Similar shifts are seen in studies using other inversion approaches, such as the
950 inversion intercomparison of Houweling et al. (2015). This result may be driven at least in part
951 by sampling and uncorrected retrieval biases in the ACOS GOSAT data set, as suggested by
952 sizable discrepancies between posterior mole fractions in the GOSAT-only inversion and surface
953 in situ and lower-tropospheric HIPPO aircraft observations. While the shift in the global sink
954 appears to be a robust feature of the inversions, the partitioning of the sink between land and
955 ocean in the inversions using either in situ or GOSAT data is found to be sensitive to prior
956 uncertainties because of negative correlations in the flux errors for the two domains. The loose
957 prior uncertainties assumed in our baseline inversions may explain the larger ocean sink
958 estimates compared to other studies, including CT2013B and the Houweling et al. (2015)
959 intercomparison. A rationale for specifying loose prior uncertainties is that this allows the
960 results to be driven more by the observations than by the prior estimates. However, in light of
961 increasing confidence in estimates of the global ocean sink (e.g. from GCP), it may be more
962 appropriate to start with a reliable set of ocean fluxes and apply tighter prior uncertainties similar
963 to those from our sensitivity test. In any case, more weight should be given to combined land
964 and ocean fluxes across latitudinal bands than to separate land and ocean flux estimates for the
965 current observational configurations.

966 The GOSAT inversion indicates significantly less CO_2 uptake in summer of 2010 than in
967 2009 in the north, consistent with a previous GOSAT analysis and likely reflecting severe heat

968 waves and drought especially across Eurasia. However, observations from the JR-STATION in
969 situ network suggest that the GOSAT inversion (and to a lesser extent, the in situ + GOSAT
970 inversion) exaggerates the 2010-2009 difference in uptake in Siberia, while the CASA-GFED
971 prior reasonably estimates that quantity. Thus, it may not be accurate to assume that year-to-year
972 posterior flux differences are insensitive to satellite retrieval biases, as was done in the other
973 study. The prior, in situ posterior, and GOSAT posterior all indicate greater CO_2 uptake over
974 North America in spring to early summer of 2010 than in 2009, consistent with wetter conditions
975 over large parts of the continent. Decreased net uptake in July-September of 2010 relative to
976 2009 in our prior appears to be consistent with record drought in the Amazon in 2010, while the
977 GOSAT inversion shows the reverse. However, time-varying biases in both the prior model and
978 the GOSAT inversion relative to Amazon aircraft profiles raise the possibility that neither one
979 correctly estimates the interannual flux difference in this region and also support the idea that
980 inversion bias can vary with data coverage. Overall, the results do demonstrate that climatic
981 conditions can drive significant year-to-year variability in natural carbon fluxes on regional
982 scales.

983 Gaps in coverage at higher latitudes, especially in winter, as well as limited sampling
984 over tropical land are a fundamental limitation of passive satellite measurements (including
985 OCO-2) and imply an important future role for active satellites such as NASA's proposed Active
986 Sensing of CO_2 Emissions over Nights, Days, and Seasons (ASCENDS) mission (Kawa et al.,
987 2010; ASCENDS Ad Hoc Science Definition Team, 2015). Ongoing development of thermal IR
988 (TIR) CO_2 retrievals for GOSAT and the future GOSAT-2 with sensitivity to several layers from
989 the lower troposphere to the lower stratosphere shows promise for producing sufficiently
990 accurate data that could also help to fill NIR retrieval coverage gaps (Saitoh et al., 2017a; b).

Additional in situ and TCCON measurements in regions that are under-observed and challenging for forward model simulations, especially Africa, would also be valuable for improving bias corrections for satellite retrievals and evaluating flux inversions using satellite data.

Competing interests

The authors declare that they have no conflict of interest.

Acknowledgments

This work has been supported by the NASA Atmospheric CO_2 Observations from Space program element and the NASA Carbon Monitoring System Program. The NASA Goddard High-End Computing Program has provided access to and assistance with supercomputing resources at the NASA Center for Climate Simulation. The ACOS GOSAT data were produced by the ACOS/OCO-2 project at the Jet Propulsion Laboratory, California Institute of Technology using spectra acquired by the GOSAT Project. We thank Chris O'Dell for providing the ACOS data to us, John Miller and Manuel Gloor for their partnership in producing the Amazonica data (with support from NERC, FAPESP, ERC, NASA, CNPQ, NOAA, IPEN, and U. of Leeds for the Amazon Greenhouse measurement program led by L. Gatti), NOAA ESRL GMD CCGG for making their flask and continuous tower data publicly available, JMA (including Yukio Fukuyama and Atsushi Takizawa) for making their in situ data publicly available on the WDCGG website and providing assistance, and Steven Wofsy for making HIPPO data available. CT2013B results are provided by NOAA ESRL, Boulder, Colorado, USA from the website at http://carbontracker.noaa.gov. Many thanks go to Martha Butler for providing inversion code

1014 and documentation. We also thank Zhengxin Zhu for contributing to data processing, Liang
1015 Feng and Paul Palmer for their inversion region map, David Baker for advice on inversions,
1016 Sander Houweling for providing results from his intercomparison paper and for helpful
1017 discussion, Lesley Ott for help with using ACOS data files and for discussions, Chris O'Dell, Ed
1018 Dlugokencky, and especially Arlyn Andrews for comments on the manuscript, and Sourish Basu
1019 for discussions.
1020

References

Andres, R. J., Boden, T. A., and Marland, G.: Monthly Fossil-Fuel CO_2 Emissions: Mass of Emissions Gridded by One Degree Latitude by One Degree Longitude, Carbon Dioxide Information Analysis Center, Oak Ridge National Laboratory, U.S. Department of Energy, Oak Ridge, Tenn., U.S.A., doi:10.3334/CDIAC/ffe.MonthlyMass.2012, 2012.

Andrews, A. E., Kofler, J., Bakwin, P. S., Zhao, C., and Tans, P.: Carbon Dioxide and Carbon Monoxide Dry Air Mole Fractions from the NOAA ESRL Tall Tower Network, 1992-2009, Version: 2011-08-31, Path: ftp://aftp.cmdl.noaa.gov/data/trace_gases/co2/in-situ/tower/, 2009.

ASCENDS Ad Hoc Science Definition Team: Active Sensing of CO_2 Emissions over Nights, Days, and Seasons (ASCENDS) Mission Science Mission Definition Study (draft), https://cce.nasa.gov/ascends_2015/ASCENDS_FinalDraft_4_27_15.pdf, 2015.

Baker, D. F., Law, R. M., Gurney, K. R., Rayner, P., Peylin, P. and co-authors: TransCom 3 inversion intercomparison: Impact of transport model errors on the interannual variability of regional CO_2 fluxes, 1988–2003, Global Biogeochem. Cycles, 20, GB1002, doi:10.1029/2004GB002439, 2006.

Baldocchi, D., et al.: FLUXNET: A new tool to study the temporal and spatial variability of ecosystem–scale carbon dioxide, water vapor, and energy flux densities, Bull. Am. Meteorol. Soc., 82, 2415–2434, 2001.

Basu, S., Guerlet, S., Butz, A., Houweling, S., Hasekamp, O., Aben, I., Krummel, P., Steele, P., Langenfelds, R., Torn, M., Biraud, S., Stephens, B., Andrews, A., and Worthy, D.: Global CO_2 fluxes estimated from GOSAT retrievals of total column CO_2, Atmos. Chem. Phys., 13, 8695–8717, doi:10.5194/acp-13-8695-2013, 2013.

1044 Belikov, D. A., Maksyutov, S., Krol, M., Fraser, A., Rigby, M., Bian, H. S., Agusti-Panareda, A.,
1045 Bergmann, D., Bousquet, P., Cameron-Smith, P., Chipperfield, M. P., Fortems-Cheiney, A.,
1046 Gloor, E., Haynes, K., Hess, P., Houweling, S., Kawa, S. R., Law, R. M., Loh, Z., Meng, L.,
1047 Palmer, P. I., Patra, P. K., Prinn, R. G., Saito, R., and Wilson, C.: Off-line algorithm for
1048 calculation of vertical tracer transport in the troposphere due to deep convection, Atmos.
1049 Chem. Phys., 13, 1093-1114, doi:10.5194/acp-13-1093-2013, 2013.
1050 Butler, M. P., Davis, K. J., Denning, A. S., and Kawa, S. R.: Using continental observations in
1051 global atmospheric inversions of CO_2: North American carbon sources and sinks, Tellus,
1052 62B, 550–572, doi:10.1111/j.1600-0889.2010.00501.x, 2010.
1053 Chatterjee, A. and Michalak, A. M.: Technical Note: Comparison of ensemble Kalman filter and
1054 variational approaches for CO_2 data assimilation, Atmos. Chem. Phys., 13, 11643–11660,
1055 doi:10.5194/acp-13-11643-2013, 2013.
1056 Chevallier, F., et al.: What eddy-covariance measurements tell us about prior land flux errors in
1057 CO_2-flux inversion schemes, Global Biogeochem. Cycles, 26, GB1021,
1058 doi:10.1029/2010GB003974, 2012.
1059 Chevallier, F., Palmer, P. I., Feng, L., Boesch, H., O'Dell, C. W., and Bousquet, P.: Toward
1060 robust and consistent regional CO_2 flux estimates from in situ and spaceborne measurements
1061 of atmospheric CO_2, Geophys. Res. Lett., 41, 1065–1070, doi:10.1002/2013GL058772,
1062 2014.
1063 Ciais, P., Rayner, P., Chevallier, F., Bousquet, P., Logan, M., Peylin, P., and Ramonet, M.:
1064 Atmospheric inversions for estimating CO_2 fluxes: methods and perspectives, Climatic
1065 Change, 103:69–92, DOI 10.1007/s10584-010-9909-3, 2010.

Connor, B. J., Bösch, H., Toon, G., Sen, B., Miller, C., and Crisp, D.: Orbiting Carbon Observatory: Inverse method and prospective error analysis, J. Geophys. Res., 113, A05305, doi:10.1029/2006JD008336, 2008.

Crisp, D.: Measuring atmospheric carbon dioxide from space with the Orbiting Carbon Observatory-2 (OCO-2), Proc. SPIE 9607, Earth Observing Systems XX, 960702, doi:10.1117/12.2187291, 2015.

Deng, F., Jones, D. B. A., Henze, D. K., Bousserez, N., Bowman, K. W., Fisher, J. B., Nassar, R., O'Dell, C., Wunch, D., Wennberg, P. O., Kort, E. A., Wofsy, S. C., Blumenstock, T., Deutscher, N. M., Griffith, D. W. T., Hase, F., Heikkinen, P., Sherlock, V., Strong, K., Sussmann, R., and Warneke, T.: Inferring regional sources and sinks of atmospheric CO_2 from GOSAT XCO_2 data, Atmos. Chem. Phys., 14, 3703–3727, doi:10.5194/acp-14-3703-2014, 2014.

Deng, F., Jones, D. B. A., O'Dell, C. W., Nassar, R., and Parazoo, N. C.: Combining GOSAT XCO_2 observations over land and ocean to improve regional CO_2 flux estimates, J. Geophys. Res. Atmos., 121, 1896–1913, doi:10.1002/2015JD024157, 2016.

Dlugokencky, E. J., Lang, P. M., Masarie, K. A., Crotwell, A. M., and Crotwell, M. J.: Atmospheric Carbon Dioxide Dry Air Mole Fractions from the NOAA ESRL Carbon Cycle Cooperative Global Air Sampling Network, 1968-2012, Version: 2013-08-28, available at: ftp://aftp.cmdl.noaa.gov/data/trace_gases/co2/flask/surface/ (last access: 18 February 2014), 2013.

Eldering, A., Wennberg, P. O., Crisp, D., Schimel, D. S., Gunson, M. R., Chatterjee, A., Liu, J., Schwandner, F. M., Sun, Y., O'Dell, C. W., Frankenberg, C., Taylor, T., Fisher, B., Osterman, G. B., Wunch, D., Hakkarainen, J., Tamminen, J., and Weir, B.: The Orbiting

Carbon Observatory-2 early science investigations of regional carbon dioxide fluxes, Science, 358, eaam5745, doi:10.1126/science.aam5745, 2017.

Engelen, R. J., Denning, A. S., and Gurney, K. R.: On error estimation in atmospheric CO_2 inversions, J. Geophys. Res., 107, 4635, doi:10.1029/2002JD002195, 2002.

Enting, I. G. and Mansbridge, J. V.: Seasonal sources and sinks of atmospheric CO_2: Direct inversion of filtered data, Tellus, 41B, 111-126, 1989.

Enting, I. G., Trudinger, C. M., and Francey, R. J.: A synthesis inversion of the concentration and $\delta^{13}C$ of atmospheric CO_2, Tellus, 47B, 35–52, 1995.

Feng, L., Palmer, P. I., Boesch, H., and Dance, S.: Estimating surface CO_2 fluxes from space-borne CO_2 dry air mole fraction observations using an ensemble Kalman Filter, Atmos. Chem. Phys., 9, 2619–2633, doi:10.5194/acp-9-2619-2009, 2009.

Feng, L., Palmer, P. I., Parker, R. J., Deutscher, N. M., Feist, D. G., Kivi, R., Morino, I., and Sussmann, R.: Estimates of European uptake of CO_2 inferred from GOSAT X_{CO2} retrievals: sensitivity to measurement bias inside and outside Europe, Atmos. Chem. Phys., 16, 1289–1302, doi:10.5194/acp-16-1289-2016, 2016.

Frankenberg, C., Kulawik, S. S., Wofsy, S., Chevallier, F., Daube, B., Kort, E. A., O'Dell, C., Olsen, E. T., and Osterman, G.: Using airborne HIAPER Pole-to-Pole Observations (HIPPO) to evaluate model and remote sensing estimates of atmospheric carbon dioxide, Atmos. Chem. Phys., 16, doi:10.5194/acp-2015-961, 2016.

Gatti, L. V., Gloor, M., Miller, J. B., Doughty, C. E., Malhi, Y., Domingues, L. G., Basso, L. S., Martinewski, A., Correia, C. S. C., Borges, V. F., Freitas, S., Braz, R., Anderson, L. O., Rocha, H., Grace, J., Phillips, O., and Lloyd, J.: Drought sensitivity of Amazonian carbon

balance revealed by atmospheric measurements, Nature, 506, 76-80, doi:10.1038/nature12957, 2014.

Gatti , L., Gloor, E., and Miller, J.: Greenhouse gas profile measurements (CO, CO_2, CH_4) above the forest canopy at four sites for the Amazonica project. NCAS British Atmospheric Data Centre, accessed 5 Dec 2016. http://catalogue.ceda.ac.uk/uuid/7201536a8b7a1a96de584e9b746acee3, 2016.

Giglio, L., Csiszar, I., and Justice, C. O.: Global distribution and seasonality of active fires as observed with the Terra and Aqua Moderate Resolution Imaging Spectroradiometer (MODIS) sensors, J. Geophys. Res., 111, G02016, doi:10.1029/2005JG000142, 2006.

Giglio, L., Randerson, J. T., van der Werf, G. R., Kasibhatla, P. S., Collatz, G. J., Morton, D. C., and DeFries, R. S.: Assessing variability and long-term trends in burned area by merging multiple satellite fire products, Biogeosciences, 7, 1171–1186, doi:10.5194/bg-7-1171-2010, 2010.

GLOBALVIEW-CO_2: Cooperative Atmospheric Data Integration Project-Carbon Dioxide, CD-ROM, NOAA-ESRL, Boulder, Colo. [Also available on Internet via anonymous FTP to ftp.cmdl.noaa.gov,Path:ccg/co2/ GLOBALVIEW], 2009.

Gourdji, S. M., Mueller, K. L., Yadav, V., Huntzinger, D. N., Andrews, A. E., Trudeau, M., Petron, G., Nehrkorn, T., Eluszkiewicz, J., Henderson, J., Wen, D., Lin, J., Fischer, M., Sweeney, C., and Michalak, A. M.: North American CO_2 exchange: intercomparison of modeled estimates with results from a fine-scale atmospheric inversion, Biogeosciences, 9, 457–475, 2012.

1132 Guerlet, S., Basu, S., Butz, A., Krol, M., Hahne, P., Houweling, S., Hasekamp, O. P., and Aben,
1133 I.: Reduced carbon uptake during the 2010 Northern Hemisphere summer from GOSAT,
1134 Geophys. Res. Lett., 40, 2378–2383, doi:10.1002/grl.50402, 2013.
1135 Gurney, K., Law, R., Rayner, P., and Denning, A. S.: TransCom 3 Experimental Protocol,
1136 Department of Atmospheric Science, Colorado State University, USA, Paper 707 (Available
1137 at http://transcom.colostate.edu/TransCom_3/transcom_3.html), 2000.
1138 Gurney, K. R., et al.: Towards robust regional estimates of CO_2 sources and sinks using
1139 atmospheric transport models, Nature, 415, 626–630, 2002.
1140 Hayes, D. J., Turner, D. P., Stinson, G., McGuire, A. D., Wei, Y., West, T. O., Heath, L. S.,
1141 deJong, B., McConkey, B. G., Birdsey, R. A., Kurz, W. A., Jacobson, A. R., Huntzinger, D.
1142 N., Pan, Y., Post, W. M., and Cook, R. B.: Reconciling estimates of the contemporary North
1143 American carbon balance among terrestrial biosphere models, atmospheric inversions, and a
1144 new approach for estimating net ecosystem exchange from inventory-based data, Global
1145 Change Biology, doi: 10.1111/j.1365-2486.2011.02627.x, 2012.
1146 Houborg, R., Rodell, M., Li, B., Reichle, R., and Zaitchik, B.: Drought indicators based on
1147 model assimilated GRACE terrestrial water storage observations, Wat. Resour. Res, 48,
1148 W07525, doi:10.1029/2011WR011291, 2012.
1149 Houweling, S., Baker, D., Basu, S., Boesch, H., Butz, A., Chevallier, F., Deng, F., Dlugokencky,
1150 E. J., Feng, L., Ganshin, A., Hasekamp, O., Jones, D., Maksyutov, S., Marshall, J., Oda, T.,
1151 O'Dell, C. W., Oshchepkov, S., Palmer, P. I., Peylin, P., Poussi, Z., Reum, F., Takagi, H.,
1152 Yoshida, Y., and Zhuravlev, R.: An intercomparison of inverse models for estimating sources
1153 and sinks of CO_2 using GOSAT measurements, J. Geophys. Res. Atmos., 120, 5253–5266,
1154 doi:10.1002/2014JD022962, 2015.

1155 Kaminski, T., Rayner, P. J., Heimann, M., and Enting, I. G.: On aggregation errors in
1156 atmospheric transport inversions, J. Geophys. Res., 106, 4703–4715, 2001.
1157 Kawa, S. R., Erickson III, D. J., Pawson, S., and Zhu, Z.: Global CO_2 transport simulations using
1158 meteorological data from the NASA data assimilation system, J. Geophys. Res., 109,
1159 D18312, doi:10.1029/2004JD004554, 2004.
1160 Kawa, S. R., Mao, J., Abshire, J. B., Collatz, G. J., Sun, X., and Weaver, C. J.: Simulation
1161 studies for a space-based CO_2 lidar mission, Tellus B, 62, 759-769, doi:10.1111/j.1600-
1162 0889.2010.00486.x, 2010.
1163 Kim, J., Kim, H. M., Cho, C.-H., Boo, K.-O., Jacobson, A. R., Sasakawa, M., Machida, T.,
1164 Arshinov, M., and Fedoseev, N.: Impact of Siberian observations on the optimization of
1165 surface CO_2 flux, Atmos. Chem. Phys., 17, doi:10.5194/acp-17-2881-2017, 2017.
1166 Kulawik, S., Wunch, D., O'Dell, C., Frankenberg, C., Reuter, M., Oda, T., Chevallier, F.,
1167 Sherlock, V., Buchwitz, M., Osterman, G., Miller, C. E., Wennberg, P. O., Griffith, D.,
1168 Morino, I., Dubey, M. K., Deutscher, N. M., Notholt, J., Hase, F., Warneke, T., Sussmann,
1169 R., Robinson, J., Strong, K., Schneider, M., De Mazière, M., Shiomi, K., Feist, D. G., Iraci,
1170 L. T., and Wolf, J.: Consistent evaluation of ACOS-GOSAT, BESD-SCIAMACHY,
1171 CarbonTracker, and MACC through comparisons to TCCON, Atmos. Meas. Tech., 9, 683–
1172 709, doi:10.5194/amt-9-683-2016, 2016.
1173 Law, R. M., et al.: TransCom model simulations of hourly atmospheric CO_2: Experimental
1174 overview and diurnal cycle results for 2002, Global Biogeochem. Cycles, 22, GB3009,
1175 doi:10.1029/2007GB003050, 2008.
1176 Le Quéré, C., Andres, R. J., Boden, T., Conway, T., Houghton, R. A., House, J. I., Marland, G.,
1177 Peters, G. P., van der Werf, G. R., Ahlström, A., Andrew, R. M., Bopp, L., Canadell, J. G.,

1178 Ciais, P., Doney, S. C., Enright, C., Friedlingstein, P., Huntingford, C., Jain, A. K., Jourdain,
1179 C., Kato, E., Keeling, R. F., Klein Goldewijk, K., Levis, S., Levy, P., Lomas, M., Poulter, B.,
1180 Raupach, M. R., Schwinger, J., Sitch, S., Stocker, B. D., Viovy, N., Zaehle, S., and Zeng, N.:
1181 The global carbon budget 1959–2011, Earth Syst. Sci. Data, 5, 165–185, doi:10.5194/essd-5-
1182 165-2013, 2013.
1183 Le Quéré, C., Moriarty, R., Andrew, R. M., Canadell, J. G., Sitch, S., Korsbakken, J. I.,
1184 Friedlingstein, P., Peters, G. P., Andres, R. J., Boden, T. A., Houghton, R. A., House, J. I.,
1185 Keeling, R. F., Tans, P., Arneth, A., Bakker, D. C. E., Barbero, L., Bopp, L., Chang, J.,
1186 Chevallier, F., Chini, L. P., Ciais, P., Fader, M., Feely, R. A., Gkritzalis, T., Harris, I., Hauck,
1187 J., Ilyina, T., Jain, A. K., Kato, E., Kitidis, V., Klein Goldewijk, K., Koven, C.,
1188 Landschützer, P., Lauvset, S. K., Lefévre, N., Lenton, A., Lima, I. D., Metzl, N., Millero, F.,
1189 Munro, D. R., Murata, A., Nabel, J., Nakaoka, S., Nojiri, Y., O'Brien, K., Olsen, A., Ono, T.,
1190 Pérez, F. F., Pfeil, B., Pierrot, D., Poulter, B., Rehder, G., Rödenbeck, C., Saito, S., Schuster,
1191 U., Schwinger, J., Séférian, R., Steinhoff, T., Stocker, B. D., Sutton, A. J., Takahashi, T.,
1192 Tilbrook, B., van der Laan-Luijkx, I. T., van der Werf, G. R., van Heuven, S., Vandemark,
1193 D., Viovy, N., Wiltshire, A., Zaehle, S., and Zeng, N.: Global Carbon Budget 2015. Earth
1194 System Science Data, 7:349-396. doi:10.5194/essd-7-349-2015, 2015.
1195 Lindqvist, H., et al.: Does GOSAT capture the true seasonal cycle of carbon dioxide?, Atmos.
1196 Chem. Phys., 15, 13023–13040, doi:10.5194/acp-15-13023-2015, 2015.
1197 Liu, J., Bowman, K. W., Lee, M., Henze, D. K., Bousserez, N., Brix, H., Collatz, G. J.,
1198 Menemenlis, D., Ott, L., Pawson, S., Jones, D., and Nassar, R.: Carbon monitoring system
1199 flux estimation and attribution: Impact of ACOS-GOSAT XCO_2 sampling on the inference of

terrestrial biospheric sources and sinks, Tellus B, 66, 22,486, doi:10.3402/tellusb.v66.22486, 2014.

Los, S. O., Collatz, G. J., Sellers, P. J., Malmström, C. M., Pollack, N. H., DeFries, R. S., Bounoua, L., Parris, M. T., Tucker, C. J., and Dazlich, D. A.: A global 9-yr biophysical land surface dataset from NOAA AVHRR data. J. Hydrometeorol., 1, 183–199, 2000.

Maksyutov, S., et al.: Regional CO_2 flux estimates for 2009–2010 based on GOSAT and ground-based CO_2 observations, Atmos. Chem. Phys., 13, 9351–9373, 2013.

Nassar, R., Jones, D. B. A., Suntharalingam, P., Chen, J. M., Andres, R. J., Wecht, K. J., Yantosca, R. M., Kulawik, S. S., Bowman, K. W., Worden, J. R., Machida, T., and Matsueda, H.: Modeling global atmospheric CO_2 with improved emission inventories and CO_2 production from the oxidation of other carbon species, Geosci. Model Dev., 3, 689–716, doi:10.5194/gmd-3-689-2010, 2010.

Niwa, Y., Machida, T., Sawa, Y., Matsueda, H., Schuck, T. J., Brenninkmeijer, C. A. M., Imasu, R., and Satoh, M.: Imposing strong constraints on tropical terrestrial CO_2 fluxes using passenger aircraft based measurements, J. Geophys. Res., 117, D11303, doi:10.1029/2012JD017474, 2012.

O'Dell, C. W., et al.: The ACOS CO_2 retrieval algorithm Part 1: Description and validation against synthetic observations, Atmos. Meas. Tech., 5, 99–121, 2012.

Olsen, S. C. and Randerson, J. T.: Differences between surface and column atmospheric CO_2 and implications for carbon cycle research, Journal of Geophysical Research, 109, D02301, doi:10.1029/2003JD003968, 2004.

1221 Orbe, C., Holzer, M., Polvani, L. M., and Waugh, D.: Air-mass origin as a diagnostic of
1222 tropospheric transport, J. Geophys. Res. Atmos., 118, 1459–1470, doi:10.1002/jgrd.50133,
1223 2013.
1224 Osterman, G., Eldering, A., Avis, C., O'Dell, C., Martinez, E., Crisp, D., Frankenberg, C., and
1225 Frankenberg, B.: ACOS Level 2 Standard Product Data User's Guide, v3.4, Jet Propulsion
1226 Laboratory, Pasadena, California, 2013.
1227 Pan, Y., Birdsey, R. A., Fang, J., Houghton, R., Kauppi, P. E., Kurz, W. A., Phillips, O. L.,
1228 Shvidenko, A., Lewis, S. L., Canadell, J. G., Ciais, P., Jackson, R. B., Pacala, S., McGuire,
1229 A. D., Piao, S., Rautiainen, A., Sitch, S., and Hayes, D.: A Large and Persistent Carbon Sink
1230 in the World's Forests, Science, 333, 988-993, doi: 10.1126/science.1201609, 2011.
1231 Parazoo, N. C., Denning, A. S., Kawa, S. R., Corbin, K. D., Lokupitiya, R. S., and Baker, I. T.:
1232 Mechanisms for synoptic variations of atmospheric CO_2 in North America, South America
1233 and Europe, Atmos. Chem. Phys., 8, 7239-7254, https://doi.org/10.5194/acp-8-7239-2008,
1234 2008.
1235 Patra, P. K., Houweling, S., Krol, M., Bousquet, P., Belikov, D., Bergmann, D., Bian, H.,
1236 Cameron-Smith, P., Chipperfield, M. P., Corbin, K., Fortems-Cheiney, A., Fraser, A., Gloor,
1237 E., Hess, P., Ito, A., Kawa, S. R., Law, R. M., Loh, Z., Maksyutov, S., Meng, L., Palmer, P.
1238 I., Prinn, R. G., Rigby, M., Saito, R., and Wilson, C.: TransCom model simulations of CH_4
1239 and related species: linking transport, surface flux and chemical loss with CH_4 variability in
1240 the troposphere and lower stratosphere, Atmos. Chem. Phys., 11, 12813–12837,
1241 doi:10.5194/acp-11-12813-2011, 2011.
1242 Peters, W., Jacobson, A. R., Sweeney, C., Andrews, A. E., Conway, T. J., Masarie, K., Miller, J.
1243 B., Bruhwiler, L. M. P., Pétron, G., Hirsch, A. I., Worthy, D. E. J., van der Werf, G. R.,

Randerson, J. T., Wennberg, P. O., Krol, M. C., and Tans, P. P.: An atmospheric perspective on North American carbon dioxide exchange: CarbonTracker, PNAS, 104, 18925-18930, 2007.

Pinzon, J. E. and Tucker, C. J.: A non-stationary 1981-2012 AVHRR $NDVI_{3g}$ time series, Remote Sensing 6, 6929-6960; doi:10.3390/rs6086929, 2014.

Randerson, J. T., Thompson, M. V., and Malmstrom, C. M.: Substrate limitations for heterotrophs: Implications for models that estimate the seasonal cycle of atmospheric CO_2, Global Biogeochem. Cycles, 10(4), 585–602, doi:10.1029/96GB01981, 1996.

Rayner, P. J., Enting, I. G., Francey, R. J., and Langenfelds, R.: Reconstructing the recent carbon cycle from atmospheric CO_2, $\delta^{13}C$ and O_2/N_2 observations, Tellus B, 51, 213–232, 1999.

Reuter, M., et al.: Satellite-inferred European carbon sink larger than expected, Atmos. Chem. Phys. Discuss., 14, 21,829–21,863, doi:10.5194/acpd-14-21829-2014, 2014.

Reuter, M., Buchwitz, M., Hilker, M., Heymann, J., Bovensmann, H., Burrows, J. P., Houweling, S., Liu, Y. Y., Nassar, R., Chevallier, F., Ciais, P., Marshall, J., and Reichstein, M.: How much CO_2 is taken up by the European terrestrial biosphere?, BAMS, 665-671, doi:10.1175/bams-d-15-00310.1, 2017.

Rienecker, M. M., Suarez, M. J., Gelaro, R., Todling, R., Bacmeister, J., Liu, E., Bosilovich, M. G., Schubert, S. D., Takacs, L., Kim, G.-K., Bloom, S., Chen, J., Collins, D., Conaty, A., Da Silva, A., Gu, W., Joiner, J., Koster, R. D., Lucchesi, R., Molod, A., Owens, T., Pawson, S., Pegion, P., Redder, C. R., Reichle, R., Robertson, F. R., Ruddick, A. G., Sienkiewicz, M., and Woollen, J.: MERRA: NASA's Modern-Era Retrospective Analysis for Research and Applications, J. Climate, 24, 3624–3648, 2011.

Rodgers, C. D.: Inverse Methods for Atmospheric Sounding: Theory and Practice, World Scientific, Singapore, 2000.

Saeki, T., Maksyutov, S., Saito, M., Valsala, V., Oda, T., Andres, R. J., Belikov, D., Tans, P., Dlugokencky, E., Yoshida, Y., Morino, I., Uchino, O., and Yokota, T.: Inverse modeling of CO_2 fluxes using GOSAT data and multi-year ground-based observations, Sci. Online Lett. Atmos., 9, 45–50, doi:10.2151/sola.2013-011, 2013a.

Saeki, T., Maksyutov, S., Sasakawa, M., Machida, T., Arshinov, M., Tans, P., Conway, T. J., Saito, M., Valsala, V., Oda, T., Andres, R. J., and Belikov, D.: Carbon flux estimation for Siberia by inverse modeling constrained by aircraft and tower CO_2 measurements, J. Geophys. Res., 118, doi:10.1002/jgrd.50127, 2013b.

Saito, R., Patra, P. K., Sweeney, C., Machida, T., Krol, M., Houweling, S., Bousquet, P., Agusti-Panareda, A., Belikov, D., Bergmann, D., Bian, H. S., Cameron-Smith, P., Chipperfield, M. P., Fortems-Cheiney, A., Fraser, A., Gatti, L. V., Gloor, E., Hess, P., Kawa, S. R., Law, R. M., Locatelli, R., Loh, Z., Maksyutov, S., Meng, L., Miller, J. B., Palmer, P. I., Prinn, R. G., Rigby, M. and Wilson, C.: TransCom model simulations of methane: Comparison of vertical profiles with aircraft measurements, J. Geophys. Res., 118, 3891-3904, doi:10.1002/jgrd.50380, 2013.

Saitoh, N., Kimoto, S., Sugimura, R., Imasu, R., Shiomi, K., Kuze, A., Niwa, Y., Machida, T., Sawa, Y., and Matsueda, H.: Bias assessment of lower and middle tropospheric CO_2 concentrations of GOSAT/TANSO-FTS TIR version 1 product, Atmos. Meas. Tech., 10, 3877–3892, doi:10.5194/amt-10-3877-2017, 2017a.

Saitoh, N., Yamada, A., Itatsu, T., Imasu, R., Shiomi, K., and Niwa, Y.: Algorithm development for the TIR bands of GOSAT-2/TANSO-FTS-2: lessons from GOSAT/TANSO-FTS TIR

CO_2 and CH_4 measurement, AGU Fall Meeting, New Orleans, US, 11-15 Dec. 2017, A33G-2472, 2017b.

Sasakawa, M., Shimoyama, K., Machida, T., Tsuda, N., Suto, H., Arshinov, M., Davydov, D., Fofonov, A., Krasnov, O., Saeki, T., Koyama, Y., and Maksyutov, S.: Continuous measurements of methane from a tower network over Siberia, Tellus B: Chemical and Physical Meteorology, 62:5, 403-416, doi:10.1111/j.1600-0889.2010.00494.x, 2010.

Sasakawa, M., Machida, T., Tsuda, N., Arshinov, M., Davydov, D., Fofonov, A., and Krasnov, O.: Aircraft and tower measurements of CO_2 concentration in the planetary boundary layer and the lower free troposphere over southern taiga in West Siberia: Long-term records from 2002 to 2011, J. Geophys. Res., doi:10.1002/jgrd.50755, 2013.

Schimel, D., Stephens, B. B., and Fisher, J. B.: Effect of increasing CO_2 on the terrestrial carbon cycle, PNAS, 112, doi/10.1073/pnas.1407302112, 2015.

Stephens, B. B., et al.: Weak northern and strong tropical land carbon uptake from vertical profiles of atmospheric CO_2, Science, 316, 1732–1735, 2007.

Takagi, H., et al.: On the benefit of GOSAT observations to the estimation of regional CO_2 fluxes, Sci. Online Lett. Atmos., 7, 161–164, 2011.

Takagi, H., et al.: Influence of differences in current GOSAT XCO_2 retrievals on surface flux estimation, Geophys. Res. Lett., 41, 2598–2605, doi:10.1002/2013GL059174, 2014.

Takahashi, T., et al.: Climatological mean and decadal change in surface ocean pCO_2, and net sea-air CO_2 flux over the global oceans, Deep Sea Res., Part II, 56(8–10), 554–577, 2009.

Tarantola, A.: Inverse problem theory: methods for data fitting and model parameter estimation, Elsevier, Amsterdam, The Netherlands, 1987.

1311 Tsutsumi, Y., Mori, K., Ikegami, M., Tashiro, T., and Tsuboi, K.: Long-term trends of
1312 greenhouse gases in regional and background events observed during 1998-2004 at
1313 Yonagunijima located to the east of the Asian continent, Atmospheric. Environment., 40,
1314 5868-5879, 2006.
1315 van der Werf, G. R., Randerson, J. T., Giglio, L., Collatz, G. J., Kasibhatla, P. S., and Arellano
1316 Jr., A. F.: Interannual variability in global biomass burning emissions from 1997 to 2004,
1317 Atmos. Chem. Phys., 6, 3423–3441, doi:10.5194/acp-6-3423-2006, 2006.
1318 van der Werf, G. R., Randerson, J. T., Giglio, L., Collatz, G. J., Mu, M., Kasibhatla, P. S.,
1319 Morton, D. C., DeFries, R. S., Jin, Y., and van Leeuwen, T. T.: Global fire emissions and the
1320 contribution of deforestation, savanna, forest, agricultural, and peat fires (1997–2009),
1321 Atmos. Chem. Phys., 10, 11707–11735, doi:10.5194/acp-10-11707-2010, 2010.
1322 van der Werf, G. R., Randerson, J. T., Giglio, L., van Leeuwen, T. T., Chen, Y., Rogers, B. M.,
1323 Mu, M., van Marle, M. J. E., Morton, D. C., Collatz, G. J., Yokelson, R. J., and Kasibhatla,
1324 P. S.: Global fire emissions estimates during 1997–2016, Earth Syst. Sci. Data, 9, 697-720,
1325 doi:10.5194/essd-9-697-2017, 2017.
1326 Wargan, K., Pawson, S., Olsen, M. A., Witte, J. C., Douglass, A. R., Ziemke, J. R., Strahan, S.
1327 E., and Nielsen, J. E.: The global structure of upper troposphere-lower stratosphere ozone in
1328 GEOS-5: A multiyear assimilation of EOS Aura data, J. Geophys. Res. Atmos., 120, 2013–
1329 2036, doi:10.1002/2014JD022493, 2015.
1330 Wofsy, S. C., et al.: HIAPER Pole-to-Pole Observations (HIPPO): fine-grained, global-scale
1331 measurements of climatically important atmospheric gases and aerosols, Philos. T. R. Soc. A,
1332 369, 2073–2086, doi:10.1098/rsta.2010.0313, 2011.

1333 Wofsy, S. C., et al.: HIPPO Merged 10-second Meteorology, Atmospheric Chemistry, Aerosol
1334 Data (R_20121129), Carbon Dioxide Information Analysis Center, Oak Ridge National
1335 Laboratory, Oak Ridge, Tennessee, U.S.A. http://dx.doi.org/10.3334/CDIAC/hippo_010
1336 (Release 20121129), 2012.
1337 Wunch, D., Wennberg, P. O., Toon, G. C., Connor, B. J., Fisher, B., Osterman, G. B.,
1338 Frankenberg, C., Mandrake, L., O'Dell, C., Ahonen, P., Biraud, S. C., Castano, R., Cressie,
1339 N., Crisp, D., Deutscher, N. M., Eldering, A., Fisher, M. L., Griffith, D. W. T., Gunson, M.,
1340 Heikkinen, P., Keppel-Aleks, G., Kyrö, E., Lindenmaier, R., Macatangay, R., Mendonca, J.,
1341 Messerschmidt, J., Miller, C. E., Morino, I., Notholt, J., Oyafuso, F. A., Rettinger, M.,
1342 Robinson, J., Roehl, C. M., Salawitch, R. J., Sherlock, V., Strong, K., Sussmann, R., Tanaka,
1343 T., Thompson, D. R., Uchino, O., Warneke, T., and Wofsy, S. C.: A method for evaluating
1344 bias in global measurements of CO_2 total columns from space, Atmos. Chem. Phys., 11,
1345 12317–12337, doi:10.5194/acp-11-12317-2011, 2011.
1346 Xu, L., Samanta, A., Costa, M. H., Ganguly, S., Nemani, R. R., and Myneni, R. B.: Widespread
1347 decline in greenness of Amazonian vegetation due to the 2010 drought, Geophys. Res. Lett.,
1348 38, L07402, doi:10.1029/2011GL046824, 2011.
1349 Yokota, T., Yoshida, Y., Eguchi, N., Ota, Y., Tanaka, T., Watanabe, H., and Maksyutov, S.:
1350 Global concentrations of CO_2 and CH_4 retrieved from GOSAT: first preliminary results,
1351 SOLA, 5, 160–163, doi:10.2151/sola.2009-041, 2009.
1352

1353 **Table 1.** Inversion Prior and Posterior Fluxes and Uncertainties Aggregated to TransCom 3 Regions, June 2009-May 2010.

TransCom Region	Prior		Fires	In Situ-Only			GOSAT-Only			In Situ + GOSAT			In Situ-Only, Tighter Prior			GOSAT-Only, Tighter Prior		
	Flux[a]	Unc	Flux	Flux	Unc	U.R. (%)[b]	Flux	Unc	U.R. (%)	Flux	Unc	U.R. (%)	Flux	Unc	U.R. (%)	Flux	Unc	U.R. (%)
Boreal North America	-0.1	0.6	0.1	0.1	0.1	81	0.2	0.3	43	0.1	0.1	87	-0.1	0.1	71	0.0	0.2	27
Temperate North America	-0.3	1.5	0.0	-0.6	0.1	93	-1.5	0.3	82	-0.7	0.1	96	-0.6	0.1	87	-1.2	0.2	71
Tropical America	0.4	1.0	0.1	-0.4	0.7	33	-0.2	0.2	79	-0.3	0.2	82	-0.2	0.3	26	-0.1	0.1	67
Temperate South America	0.4	1.2	0.1	0.4	0.8	31	1.1	0.2	85	1.0	0.2	85	0.3	0.3	27	0.9	0.1	73
Northern Africa	0.2	1.1	0.4	1.5	0.7	38	2.0	0.2	83	1.8	0.2	84	1.1	0.3	28	2.0	0.1	70
Southern Africa	0.0	1.2	0.8	-0.1	0.7	44	-0.6	0.1	89	-0.5	0.1	89	-0.1	0.3	38	-0.6	0.1	80
Boreal Asia	-0.1	1.2	0.1	-1.2	0.4	70	-0.5	0.4	65	-1.2	0.2	87	-1.0	0.2	60	-0.5	0.2	51
Temperate Asia	0.0	1.8	0.1	-0.1	0.7	61	1.4	0.4	79	0.9	0.3	85	-0.5	0.3	53	1.0	0.2	67
Tropical Asia	0.3	0.6	0.4	0.0	0.4	33	0.5	0.3	54	0.7	0.2	61	0.4	0.2	25	0.8	0.1	39
Australia	0.0	0.5	0.1	-0.2	0.4	15	0.6	0.2	71	0.3	0.1	73	-0.2	0.2	12	0.3	0.1	56
Europe	-0.1	1.3	0.0	0.6	0.4	70	-1.5	0.3	75	-0.6	0.2	87	0.3	0.2	61	-1.6	0.2	64
North Pacific Ocean	-0.5	0.3	0.0	-0.9	0.1	51	-0.5	0.2	29	-1.1	0.1	67	-0.8	0.1	29	-0.5	0.1	11
Tropical West Pacific Ocean	0.1	0.3	0.0	0.1	0.2	26	0.3	0.1	51	0.5	0.1	59	0.1	0.1	15	0.3	0.1	24
Tropical East Pacific Ocean	0.4	0.3	0.0	0.4	0.2	25	0.4	0.1	54	0.3	0.1	62	0.4	0.1	13	0.4	0.1	25
South Pacific Ocean	-0.3	0.6	0.0	-1.0	0.4	32	-1.1	0.3	51	-1.8	0.2	60	-0.6	0.2	18	-0.9	0.1	30
Arctic/Northern Ocean	-0.3	0.3	0.0	-0.4	0.1	56	-0.5	0.2	19	-0.1	0.1	62	-0.3	0.1	31	-0.4	0.1	5
North Atlantic Ocean	-0.2	0.2	0.0	-0.8	0.1	35	-0.5	0.1	23	-1.0	0.1	50	-0.5	0.1	12	-0.3	0.1	6
Tropical Atlantic Ocean	0.1	0.3	0.0	0.1	0.2	23	0.3	0.2	42	0.4	0.1	56	0.1	0.1	9	0.2	0.1	14
South Atlantic Ocean	-0.2	0.4	0.0	-0.5	0.3	19	-0.7	0.2	38	-1.0	0.2	49	-0.3	0.1	8	-0.5	0.1	18
Southern Ocean	-0.2	0.6	0.0	-0.4	0.3	48	-0.9	0.4	41	0.2	0.2	62	-0.5	0.1	34	-1.1	0.1	22
Tropical Indian Ocean	0.1	0.4	0.0	0.0	0.3	27	0.7	0.2	56	0.5	0.2	62	0.1	0.1	16	0.4	0.1	32
Southern Indian Ocean	-0.4	0.3	0.0	-0.5	0.2	15	-0.6	0.2	29	-0.6	0.2	40	-0.5	0.1	7	-0.4	0.1	11

[a]Fluxes in table, in Pg C, include fires but not fossil emissions

[b]Uncertainty reduction

1354 **Table 2.** Normalized Cost Function Values for the Inversions.

Inversion	**A Priori**	**A Posteriori**
In situ only	112.4	4.0
GOSAT only	2.2	0.8
In situ + GOSAT	12.2	1.1
In situ only, decreased prior uncertainties	112.4	5.0
GOSAT only, decreased prior uncertainties	2.2	0.8

1355

1356

Table 3. Mean 2010-2009 difference in mole fractions over June-July-August at Siberian sites (in ppm).

Site	Observations	Prior	GOSAT-Only Post	In Situ + GOSAT Post	Prior - Obs	(GOSAT-Only) - Obs	(In Situ + GOSAT) - Obs
VGN	5.2	5.3	7.4	6.6	0.1	2.2	1.4
AZV	7.0	6.3	8.1	7.1	-0.7	1.1	0.1
SVV	2.6	4.0	3.4	4.6	1.4	0.8	2.0
IGR	4.9	5.7	5.1	4.6	0.8	0.2	-0.3
KRS	6.6	5.4	3.8	3.2	-1.2	-2.8	-3.4
YAK	2.1	2.5	4.2	2.5	0.4	2.1	0.4

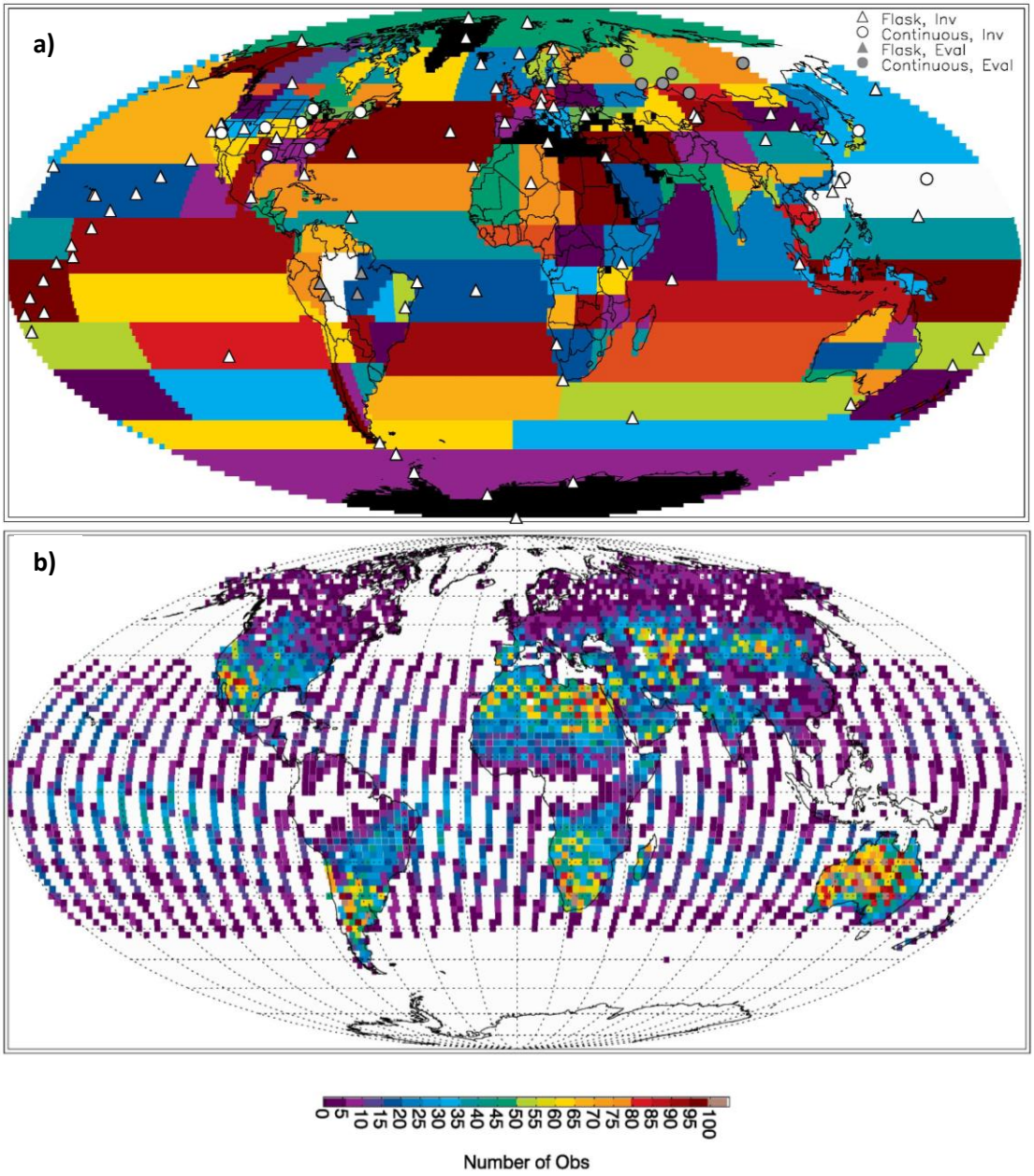

1360

1361 **Figure 1.** Locations of a) in situ observation sites and b) GOSAT XCO_2 observations used in the

1362 inversions. Also shown in a) are the 108 flux regions. Flask and continuous measurement sites

1363 in a) are represented by different symbols, and sites used in inversions and in their evaluation are

1364 represented by different colors. Observations in b) correspond to the ACOS B3.4 retrieval, are

filtered and averaged over each hour and 2° x 2.5° PCTM model grid column, and are shown for June 2009-May 2010.

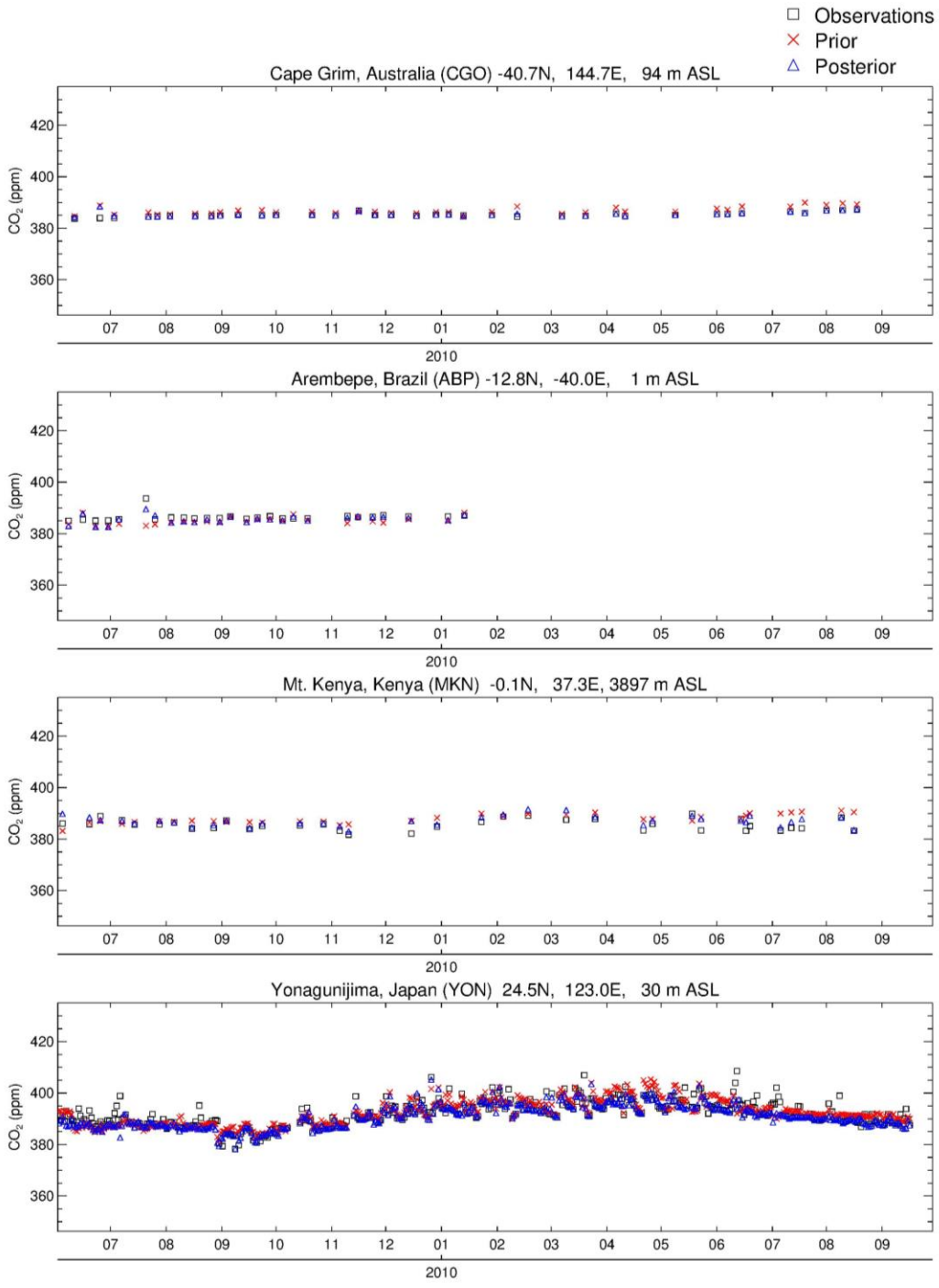

1367

1368 **Figure 2.** Comparison of model and observed time series of CO_2 mole fractions at selected

1369 surface sites. Posterior mole fractions are for the in situ-only inversion. Sites are arranged from

1370 south to north. Elevations include intake heights on towers where applicable.

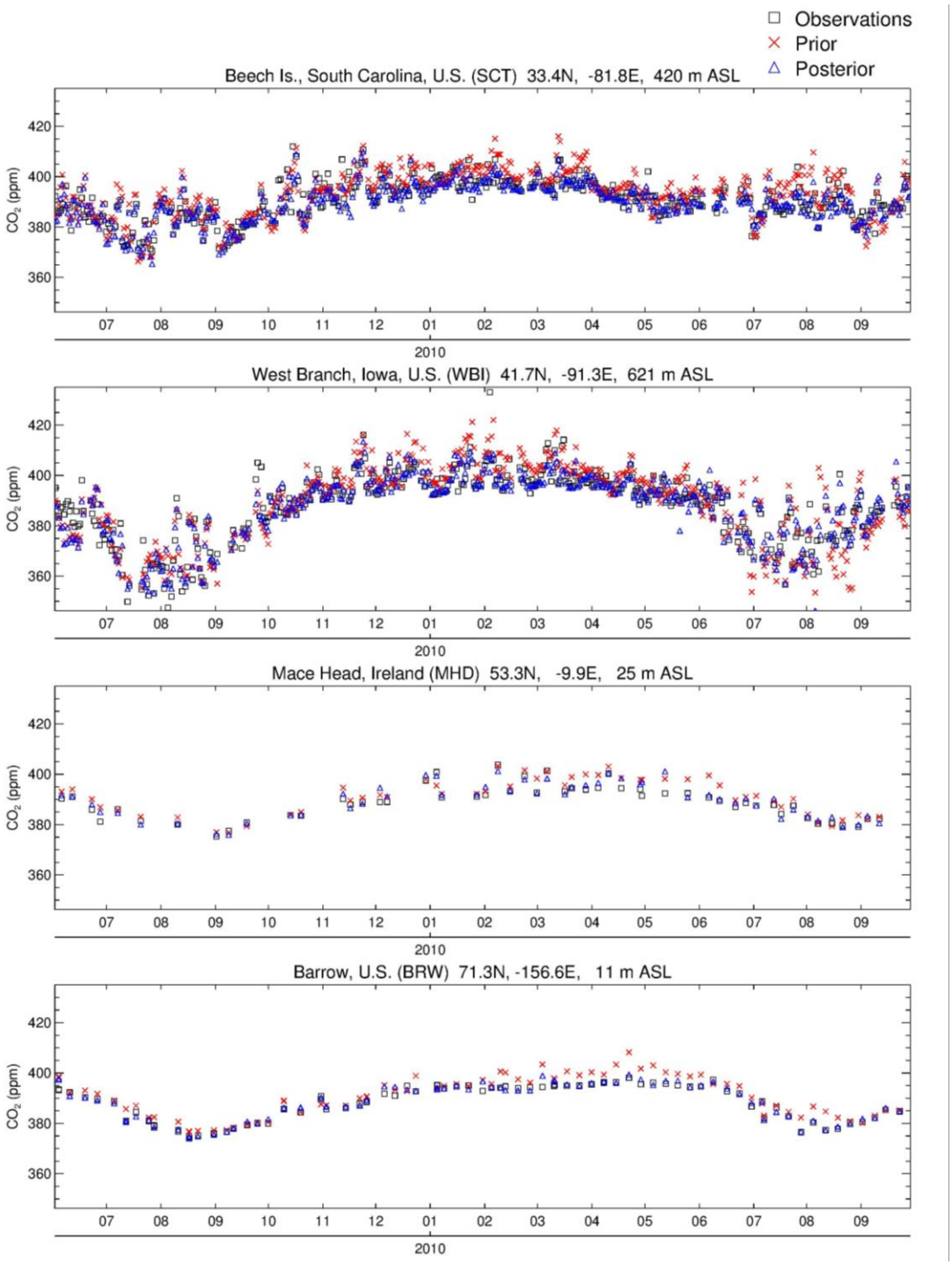

1371

1372 **Figure 2.** (continued)

1373

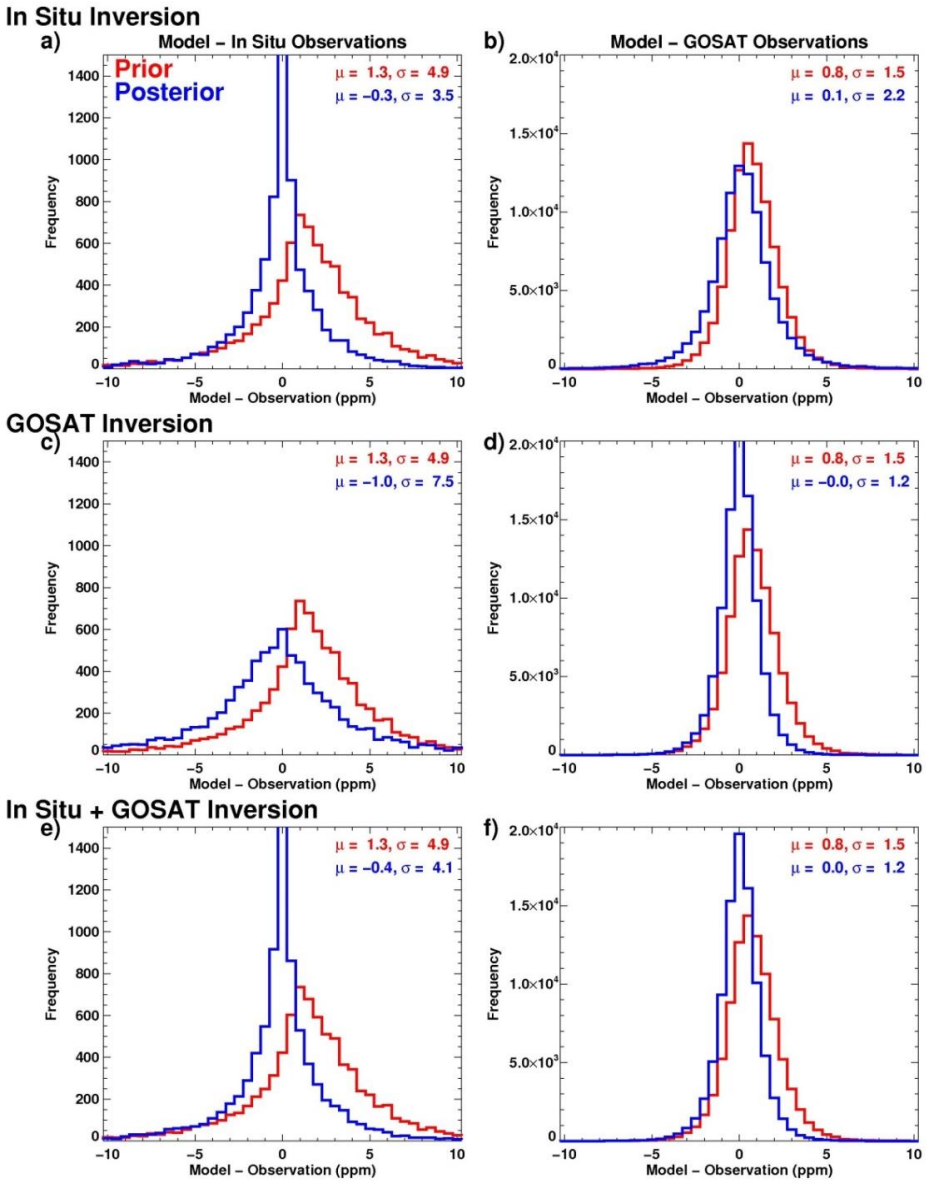

Figure 3. Full comparison of model and observations. Model-observation difference histograms are shown for (a) in situ-only inversion and in situ observations, (b) in situ-only inversion and GOSAT observations, (c) GOSAT-only inversion and in situ observations, (d) GOSAT-only inversion and GOSAT observations, (e) in situ + GOSAT inversion and in situ observations, and (f) in situ + GOSAT inversion and GOSAT observations. Mean differences and standard deviations are indicated in the panels.

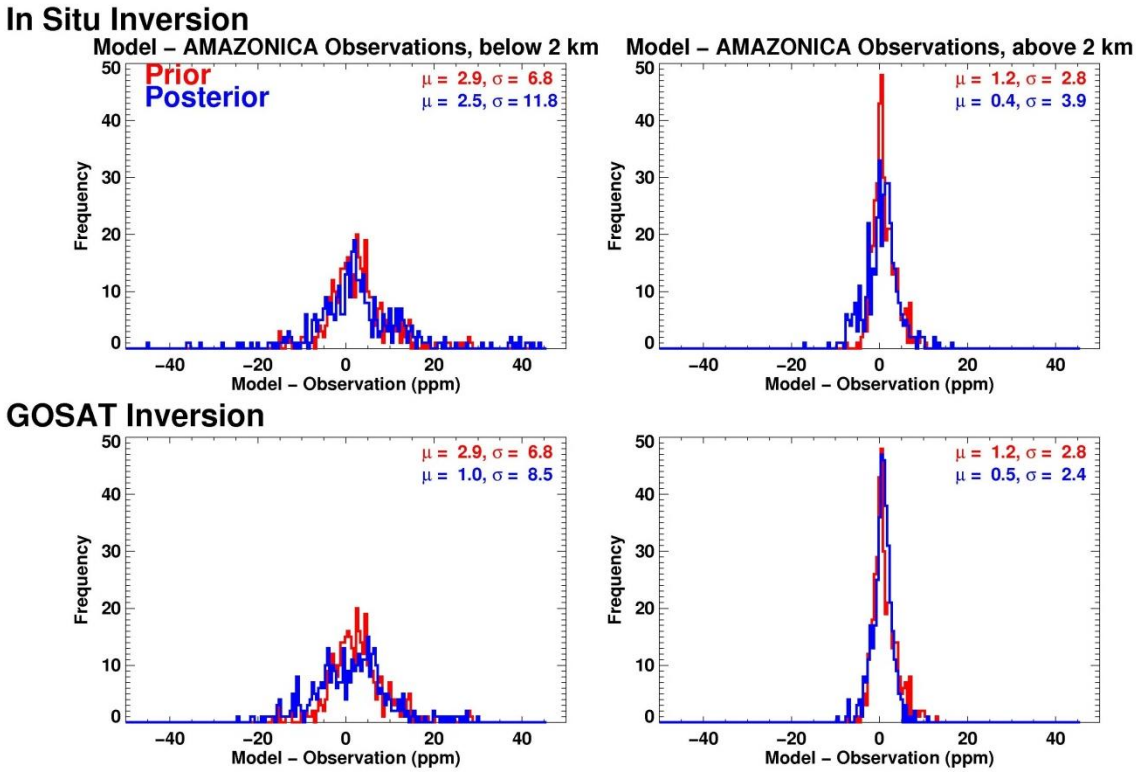

Figure 4. Comparison of model and Amazon aircraft observations (Amazonica project) over the period of overlap, Jan.-Sep. 2010. Top two panels show model-observation difference histograms for the in situ-only inversion and bottom two panels show results for the GOSAT-only inversion. Comparisons are shown separately for model and data below 2 km altitude (left) and above 2 km (right). Mean differences and standard deviations are indicated in the panels.

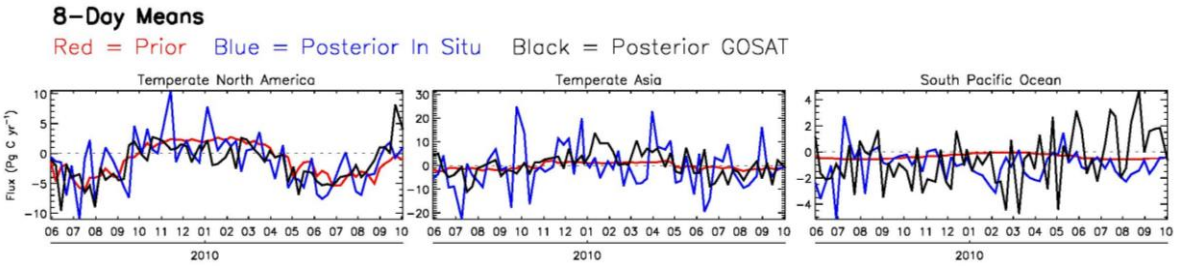

1388

1389 **Figure 5.** Prior, posterior in situ-only, and posterior GOSAT-only 8-day mean NEP (× -1) and

1390 ocean fluxes, aggregated over selected TransCom regions. Note that vertical scales are different

1391 in each of the panels.

1392

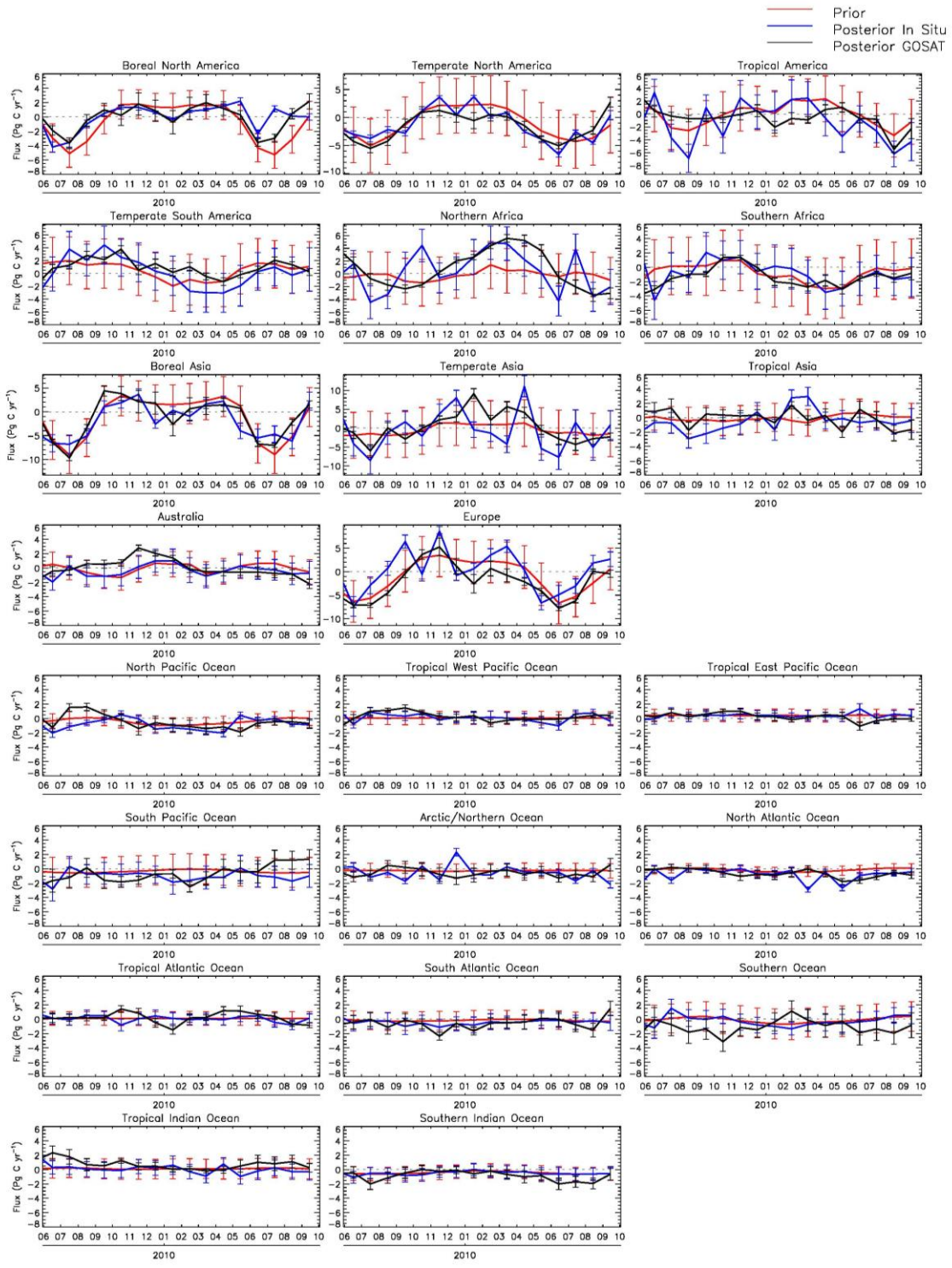

Figure 6. Same as Fig. 5, except showing monthly means of fluxes for all TransCom regions, with error bars that represent 1σ uncertainties.

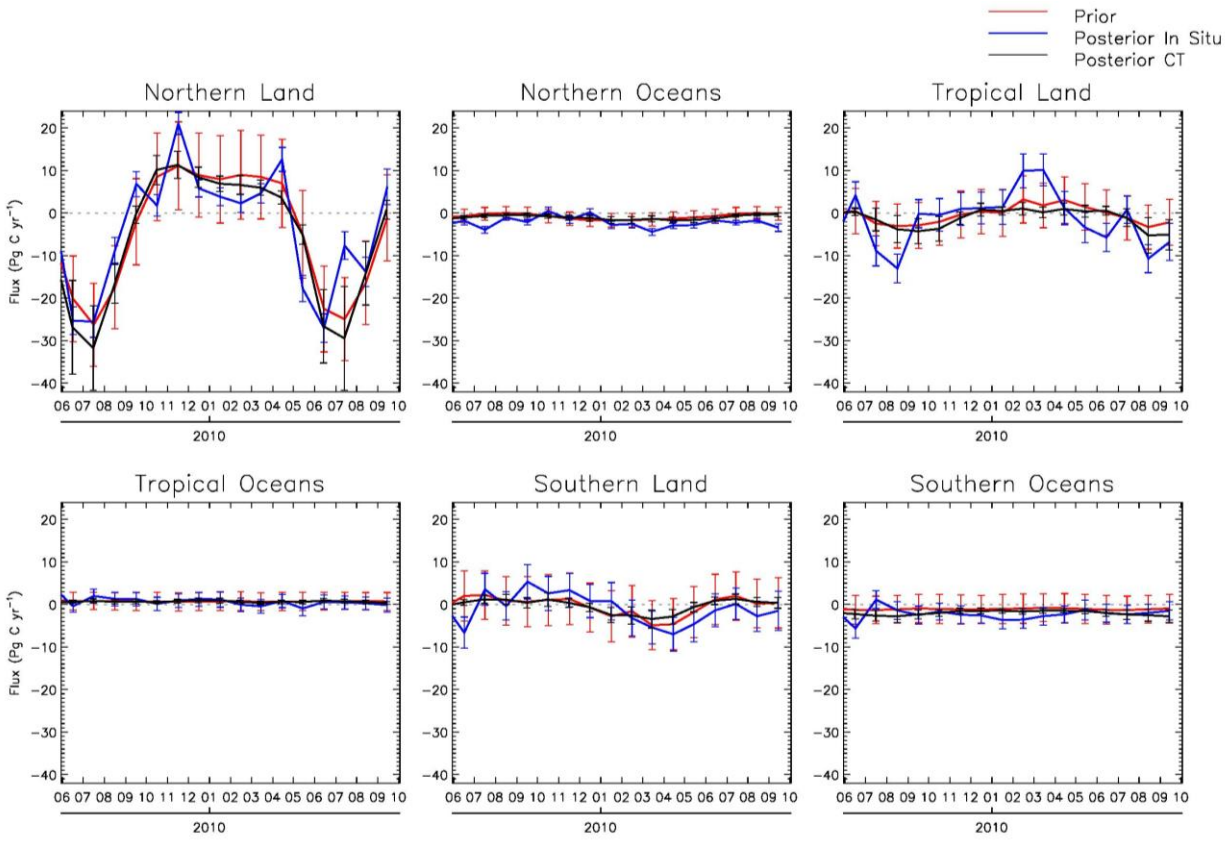

Figure 7. Comparison of our in situ-only inversion monthly mean NEP (× -1) and ocean fluxes, aggregated over large regions (as defined in TC3), with posterior fluxes from NOAA's CarbonTracker (CT2013B) data assimilation system. The priors shown are from our analysis; CT2013B priors are similar. Error bars represent 1σ uncertainties.

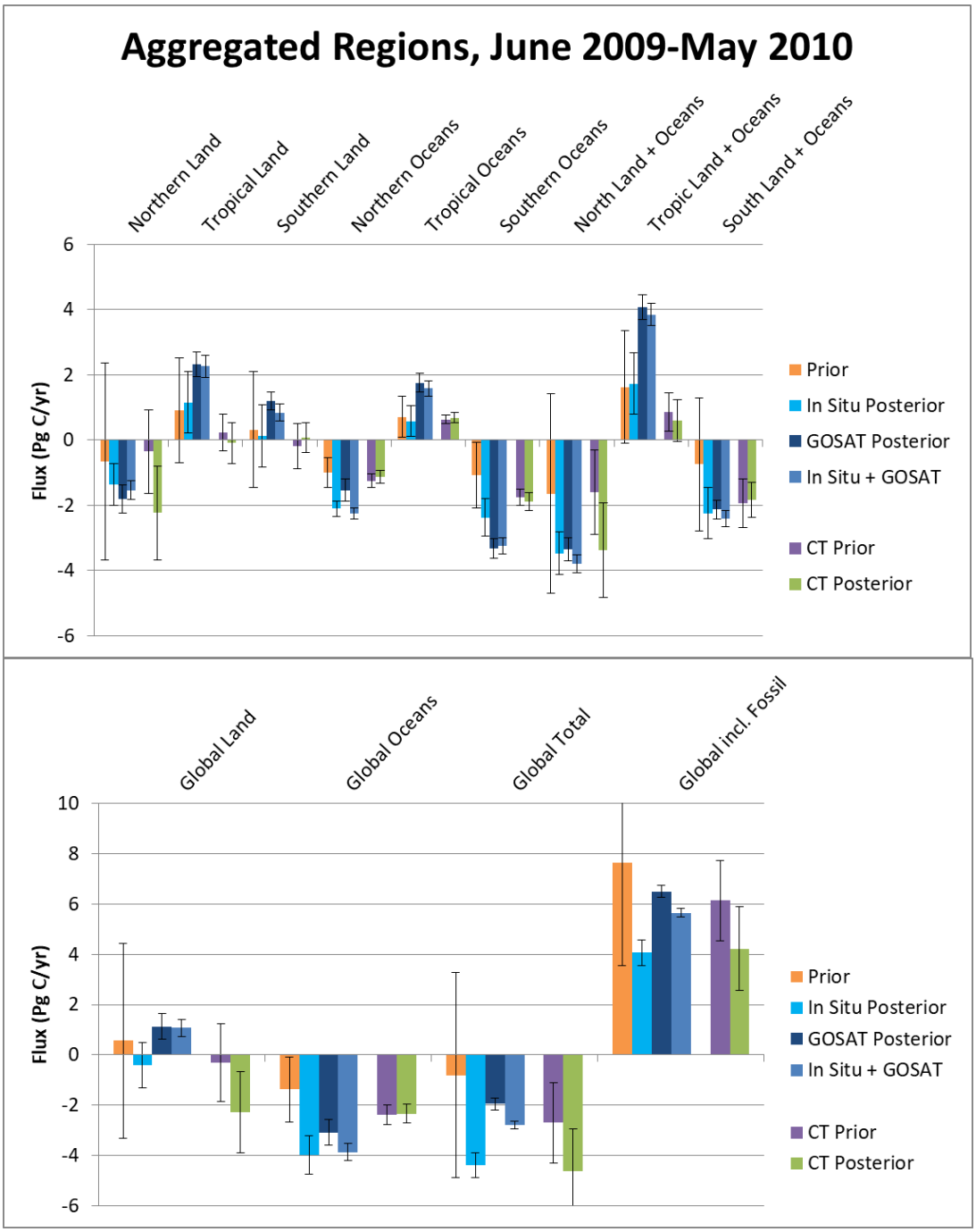

1403

1404

1405 **Figure 8.** Twelve-month mean NEP (× -1), fire, and ocean fluxes aggregated over large regions.

1406 Included are results for the in situ-only, GOSAT-only, and in situ + GOSAT inversions as well

1407 as priors. Shown for comparison are priors and posteriors from CT2013B. Error bars represent

1408 1σ uncertainties; for CT2013B, "external" (across a set of priors) as well as "internal" (within a

1409 particular inversion) uncertainties are included. In summing monthly CT2013B fluxes over the
1410 12 months, we assumed zero error correlation between months.
1411

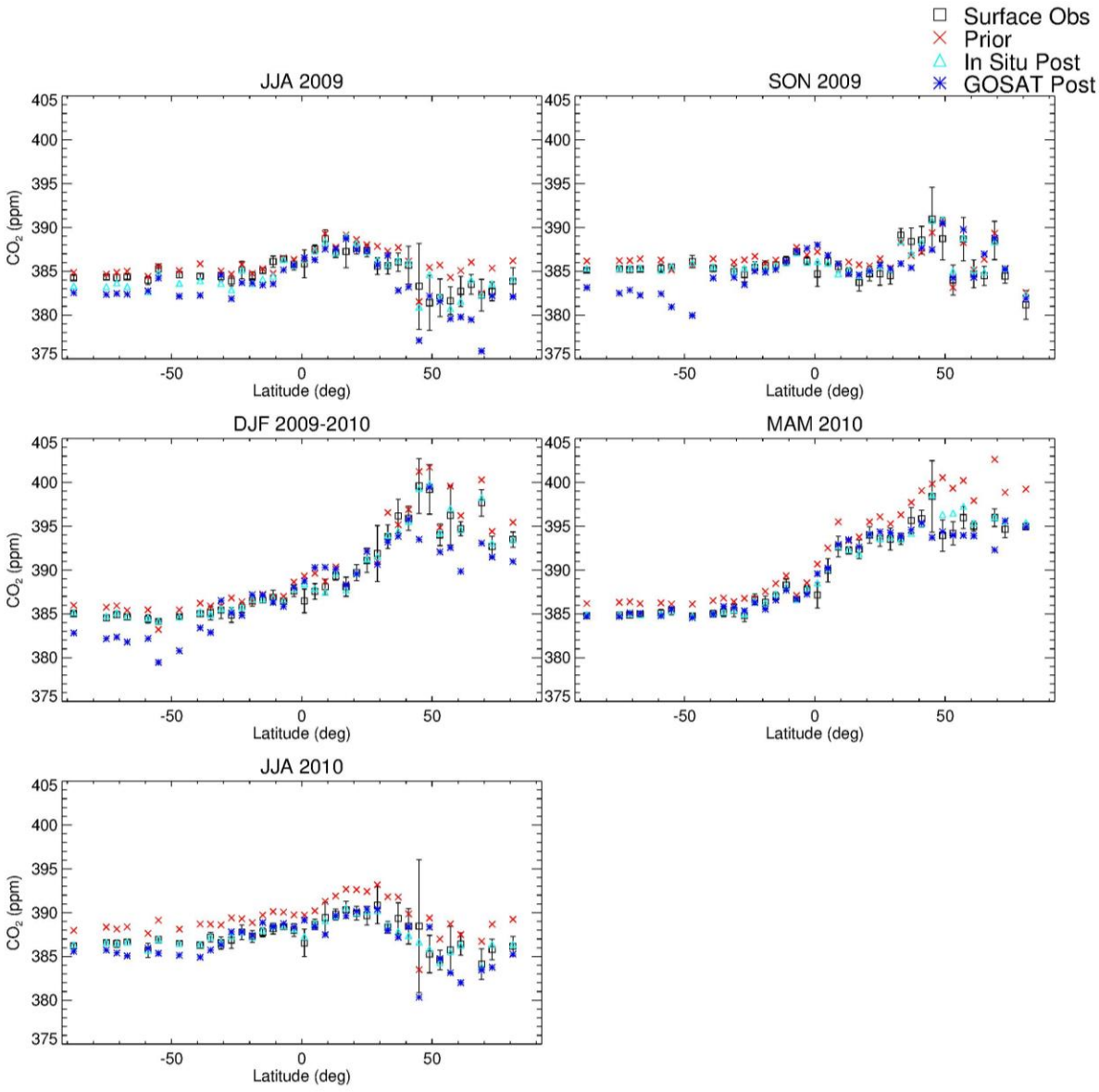

Figure 9. Latitudinal profiles of seasonal mean CO_2 mole fractions at surface sites for observations, prior, in situ-only posterior, and GOSAT-only posterior. Values are averaged in 4° bins. Error bars account for the spread of the observations within each season and bin as well as the uncertainty of each observation.

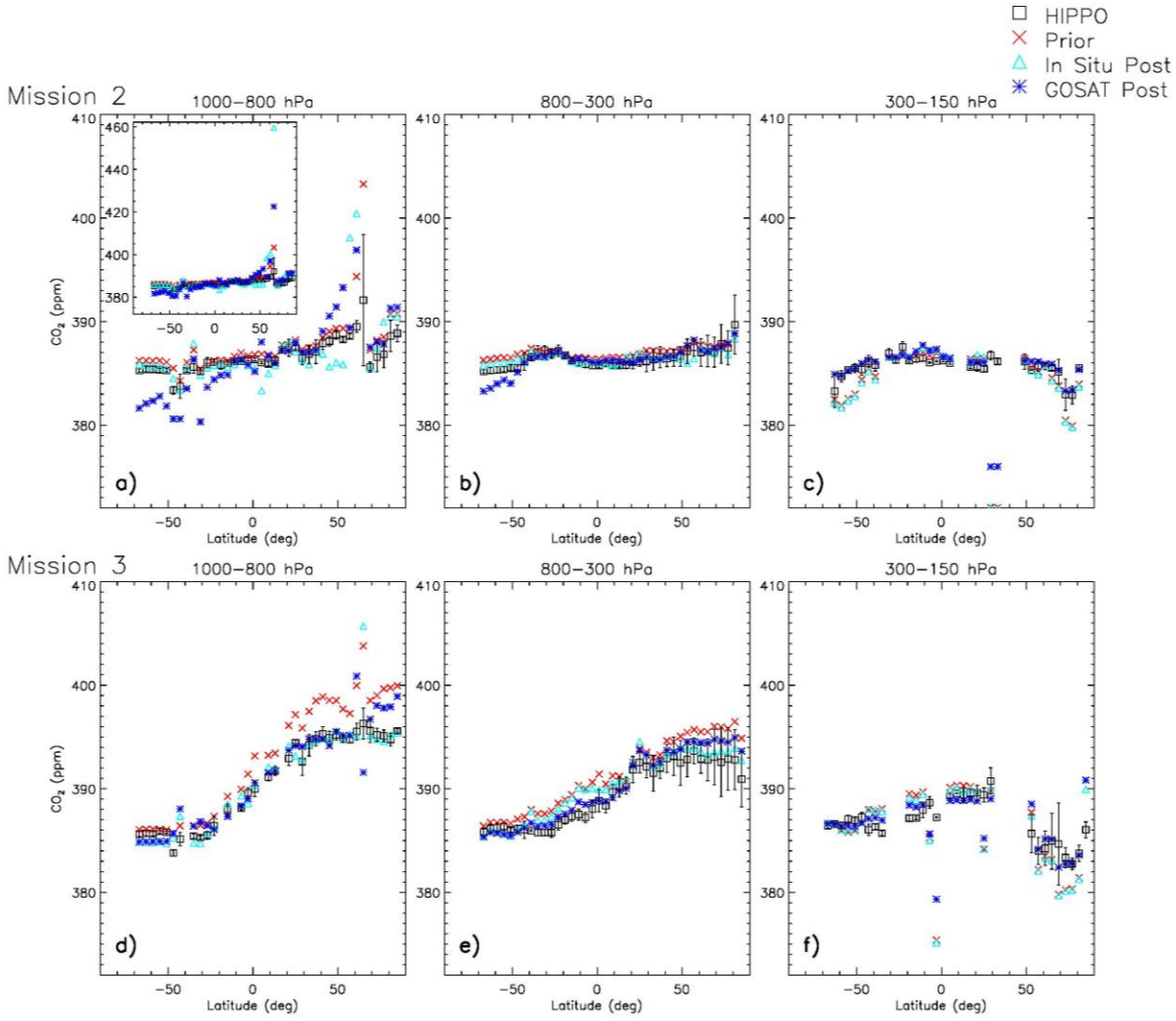

Figure 10. Latitudinal profiles of CO_2 mole fractions for HIPPO observations and co-sampled prior, in situ-only posterior, and GOSAT-only posterior. Mission 2 took place during Oct 31-Nov 22, 2009; Mission 3 took place Mar 24-Apr 16, 2010. Values are averaged in three altitude bins and 4° latitude bins. The inset in the first panel contains an expanded y-axis range that shows two points that do not fit into the default range. Flight segments over the temperate North American continent (east of -130°) are excluded from this comparison in order to focus on the Pacific. Error bars represent the standard deviations of the observations within each bin.

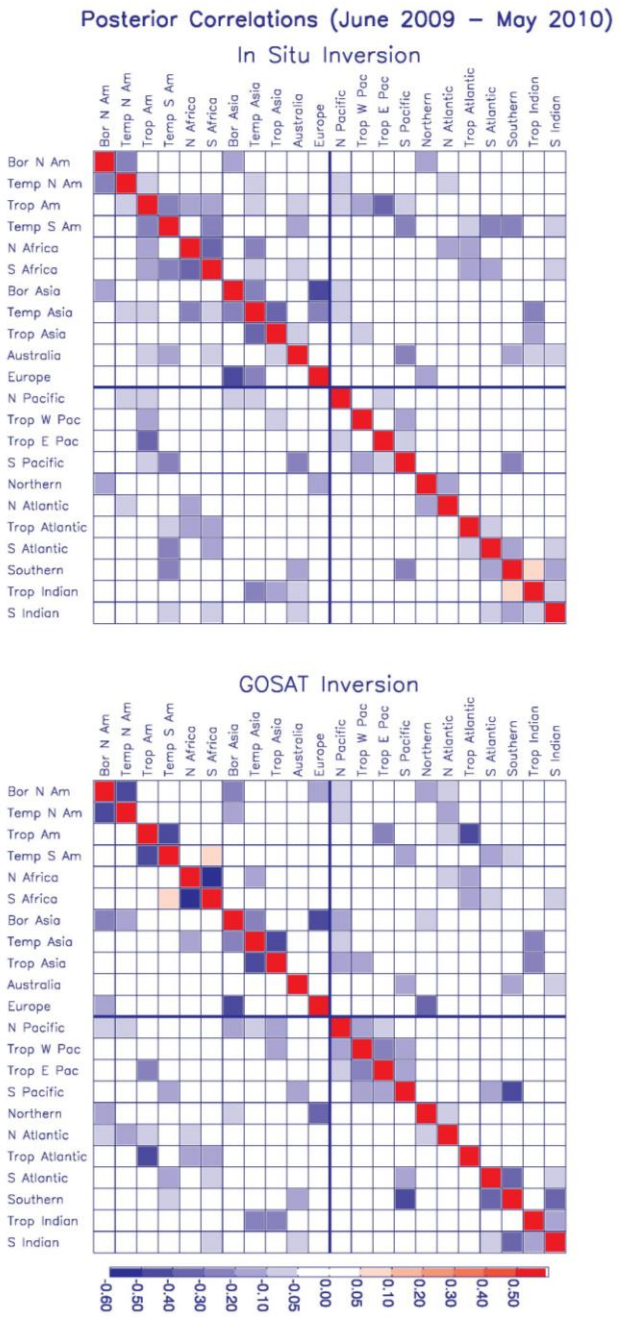

1425

1426 **Figure 11.** Posterior flux error correlations, aggregated to TC3 regions and a 12-month period,
1427 for (a) the in situ-only inversion, and (b) the GOSAT-only inversion. The correlation is equal to
1428 the error covariance divided by the product of the corresponding flux uncertainties (σ). Values
1429 on the main diagonal are equal to 1.

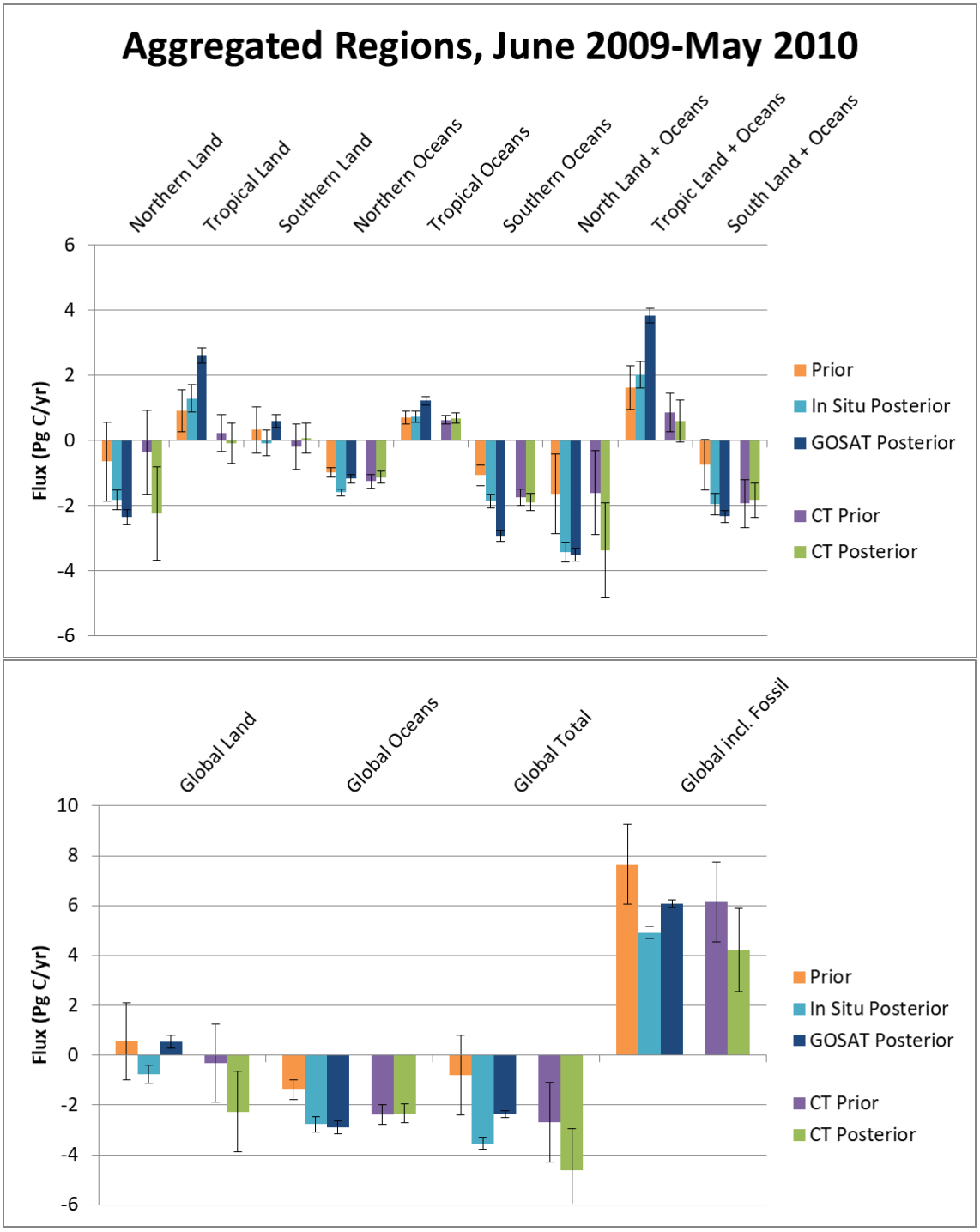

Figure 12. Similar to Fig. 8, except showing results for inversions with tighter prior constraints (with prior uncertainties similar to CarbonTracker's). Included are results for the in situ-only

and GOSAT-only inversions. CT2013B results shown in Fig. 8 are repeated here. Error bars represent 1σ uncertainties.

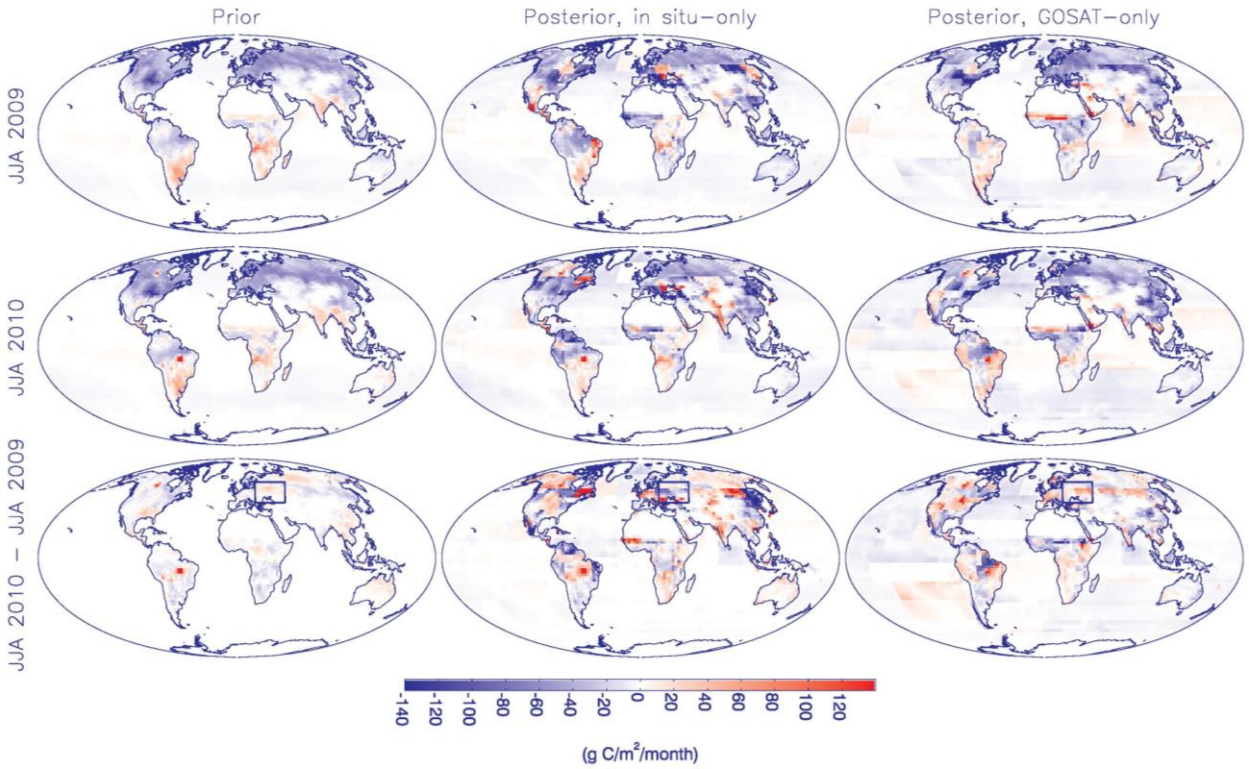

Figure 13. Comparison of spatial distribution of fluxes for June-July-August of 2010 vs. 2009. Included are natural and fire fluxes. Shown are fluxes for 2009 (top), 2010 (middle), and the 2010-2009 difference (bottom), for the priors (left), in situ-only inversion (middle), and GOSAT-only inversion (right). In the bottom row, boxes enclose the region around western Russia where there were intense heat waves, severe drought, and extensive fires. Note that the grid-scale spatial variability shown is not optimized in the inversions, so only patterns at the scale of the 108 flux regions contain information from the observations.

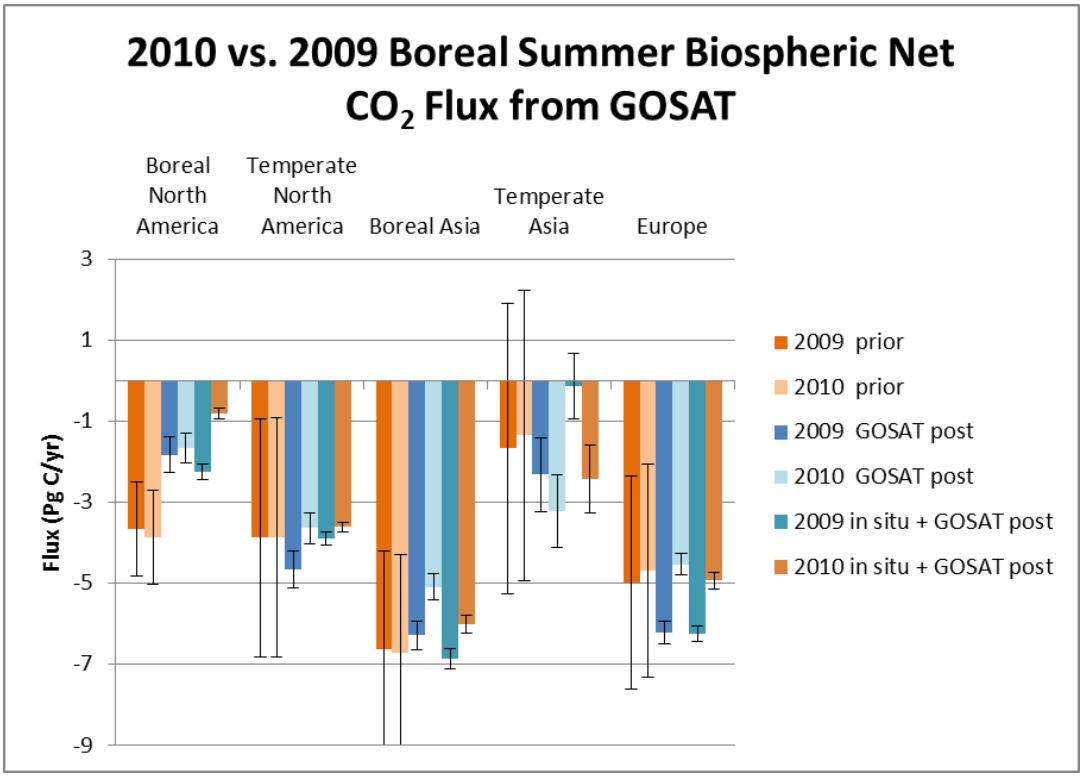

1447

1448 **Figure 14.** Comparison of prior, GOSAT-only posterior, and in situ + GOSAT posterior fluxes

1449 aggregated over northern regions for June-July-August of 2010 vs. 2009. Included are NEP (× -

1450 1) and fire fluxes. Error bars represent 1σ uncertainties.

1451

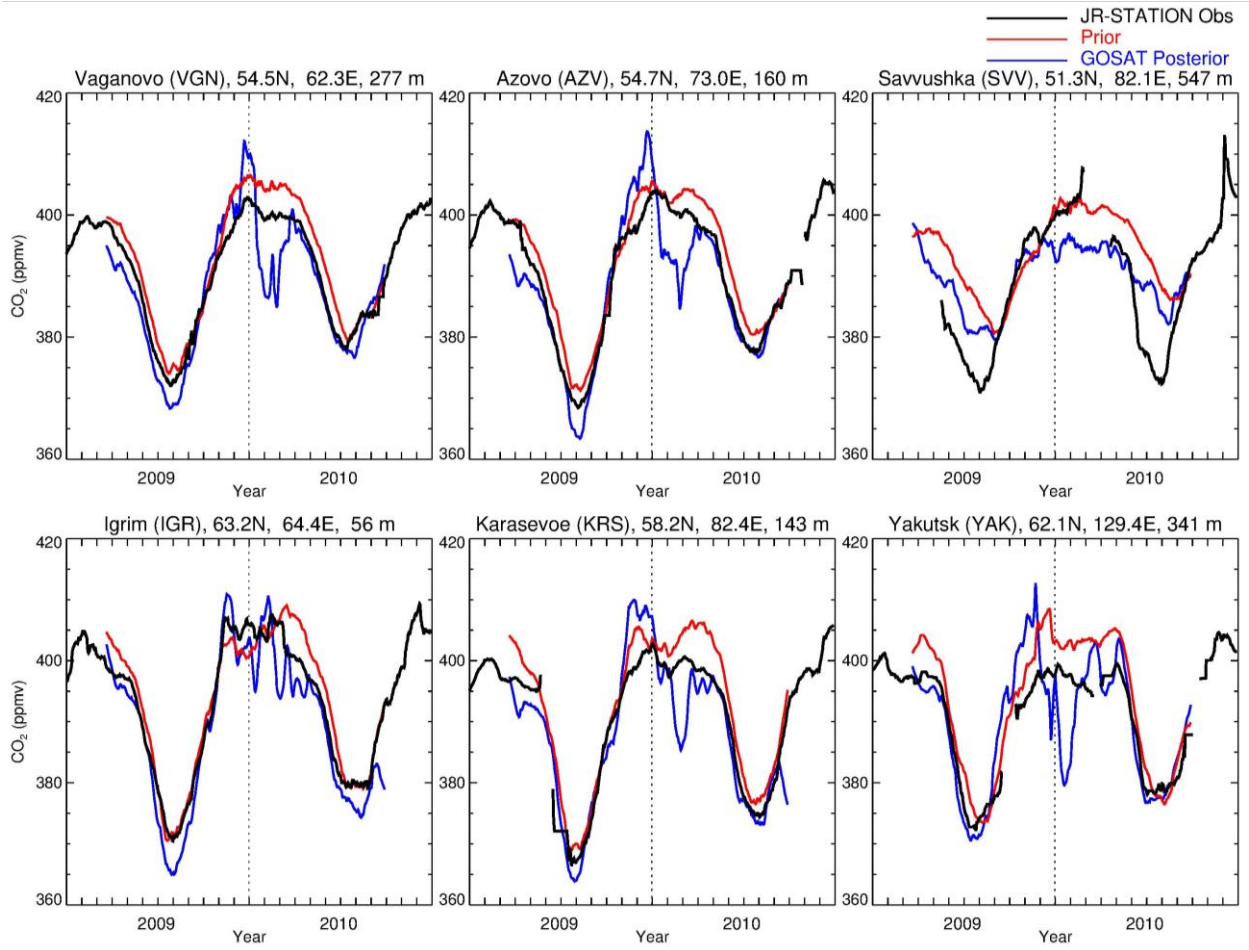

Figure 15. Evaluation of the prior model and GOSAT-only inversion against JR-STATION in situ observations in Siberia. Shown are daily afternoon average (1200-1700 local time) mole fractions from the highest level on each tower, the time series of which are smoothed with a 31-day window. Sites are arranged from west to east, first at lower latitudes and then at higher latitudes, excluding those with data gaps in the summer. Elevations shown include intake heights on towers.